Cell Reports

Resource

Custom affinity probes reveal DNA-damage-induced, ssDNA-independent chromatin SUMOylation in budding yeast

Graphical abstract

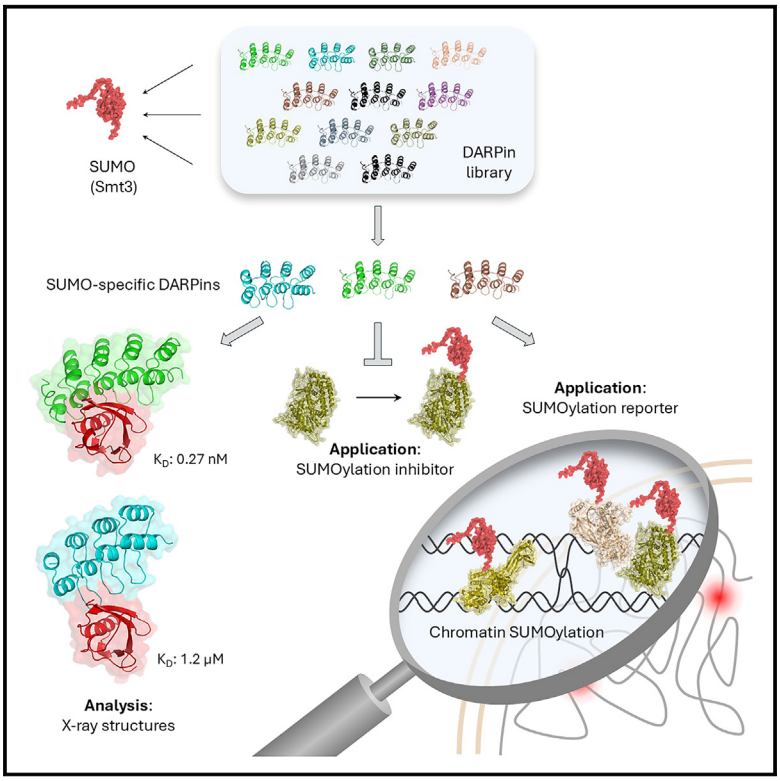

Highlights

- DARPin-based affinity probes were selected against the budding yeast SUMO (Smt3)
- Structural analyses reveal unique interaction modes with Smt3's SIM-binding region
- DARPins can serve as compartment-specific inhibitors or neutral SUMOylation sensors
- DARPins reveal DNA-damage-induced, Mms21-mediated chromatin SUMOylation

Authors

Vera Tröster, Ronald P. Wong, Arne Börgel, ..., Andreas Plückthun, Eva Wolf, Helle D. Ulrich

Correspondence

h.ulrich@imb-mainz.de

In brief

Tröster et al. report the isolation as well as biochemical and structural characterization of DARPin-based affinity probes directed against the posttranslational modifier SUMO from budding yeast. Application as *in vivo* biosensors reveals Mms21-mediated chromatin SUMOylation in response to DNA damage, associated with homologous recombination but independent of single-stranded DNA.

Tröster et al., 2025, Cell Reports *44*, 115353
March 25, 2025
https://doi.org/10.1016/j.celrep.2025.115353

CellPress

Cell Reports

CellPress
OPEN ACCESS

Resource

Custom affinity probes reveal DNA-damage-induced, ssDNA-independent chromatin SUMOylation in budding yeast

Vera Tröster,[1,4,6] Ronald P. Wong,[1,6] Arne Börgel,[2] Baris Cakilkaya,[2] Christian Renz,[1] Martin M. Möckel,[1] Karolin Eifler-Olivi,[1] Joana Marinho,[3] Thomas Reinberg,[3] Sven Furler,[3] Jonas V. Schaefer,[3,5] Andreas Plückthun,[3] Eva Wolf,[2] and Helle D. Ulrich[1,7,*]

[1]Institute of Molecular Biology (IMB) gGmbH, 55128 Mainz, Germany
[2]Institute of Molecular Physiology, Johannes Gutenberg University, 55128 Mainz, Germany
[3]Department of Biochemistry, University of Zurich, 8057 Zurich, Switzerland
[4]Present address: Interdisciplinary Centre for Research, Graduate Support and Human Resource Development, University of Koblenz, 56070 Koblenz, Germany
[5]Present address: CSL Behring AG, 3014 Bern, Switzerland
[6]These authors contributed equally
[7]Lead contact
*Correspondence: h.ulrich@imb-mainz.de
https://doi.org/10.1016/j.celrep.2025.115353

SUMMARY

The small ubiquitin-related modifier SUMO regulates cellular processes in eukaryotes either by modulating individual protein-protein interactions or with relaxed substrate selectivity by group modification. Here, we report the isolation and characterization of designed ankyrin repeat protein (DARPin)-based affinity probes directed against budding yeast SUMO (Smt3). We validate selected DARPins as compartment-specific inhibitors or neutral detection agents. Structural characterization reveals a recognition mode distinct from that of natural SUMO interactors. *In vivo* application pinpoints Smt3's essential function to the nucleus and demonstrates DARPin-mediated sensitization toward various stress conditions. A subset of selected clones is validated as SUMOylation reporters in cells. In this manner, we identify a DNA-damage-induced nuclear SUMOylation response that—in contrast to previously reported chromatin group SUMOylation—is independent of single-stranded DNA and the SUMO-E3 Siz2 but depends on Mms21 and likely reflects late intermediates of homologous recombination. Thus, Smt3-specific DARPins can provide insight into the dynamics of SUMOylation in defined subcellular structures.

INTRODUCTION

The essential small ubiquitin-like modifier, SUMO, contributes to a variety of cellular pathways in eukaryotes, ranging from transcription regulation, cell division, and nuclear import and export to DNA repair, protein turnover, and the cellular stress response.[1,2] While fungi, nematodes, and fruit flies express a single gene encoding SUMO (called *SMT3* in these organisms), human cells harbor multiple paralogs, of which SUMO2 and SUMO3 share 97% identity. SUMO is covalently attached to its targets by an enzymatic cascade comprising a heterodimeric activating enzyme (E1), a single conjugating enzyme (E2), Ubc9, and a limited set of SUMO-specific protein ligases (E3s).

The functions of SUMO are generally mediated via protein-protein interactions. Beyond defined, stoichiometric interactions, SUMO engages in a phenomenon known as group modification, wherein the protein acts in a glue-like manner, modifying multiple subunits of complexes or larger surfaces and thereby establishing multivalent interaction networks.[3] Here, the identity of the substrates is less critical than their contributions to specific macromolecular assemblies, condensates, or pathways. In most cases, SUMO binding partners associate via so-called SUMO interaction motifs (SIMs).[4,5] Although SIMs follow a relatively relaxed consensus motif and usually exhibit weak binding affinities, with dissociation constants (K_D) above 1 μM, their mode of interaction with SUMO is surprisingly well conserved. SIMs are short linear peptides with a hydrophobic core flanked on one side by one or more acidic residues. The peptide contacts a groove between the α helix and the β sheet of SUMO's β-grasp fold. By doing so, the SIM aligns with the β sheet in a parallel or antiparallel manner. Its affinity is governed predominantly by hydrophobic and some electrostatic side-chain interactions. Interaction studies and proteomic screens[6–9] demonstrate that some SIM-containing SUMO interactors exhibit a preference for either SUMO1 or SUMO2/3, likely mediated by residues adjacent to the canonical SUMO-SIM interaction patch.

Insight into the actions of SUMO in cells is facilitated by inhibitors and specific analytical tools. Inhibitors directed against

SUMO-E1, SUMO-E2, and several isopeptidases are available,[10,11] and antibodies against SUMO have been instrumental in identifying SUMO conjugates from various organisms.[12,13] In budding yeast, the use of inhibitors is often problematic because of the cells' capacity to reject foreign substances. Instead, a temperature-sensitive mutant of Ubc9 has served as a genetic tool to inhibit SUMOylation.[14] For the purpose of tracking or inhibiting proteins *in vivo*, small synthetic binding proteins have often proven superior to antibodies.[15] Two different sets of binders directed against human SUMO paralogs, based on the monobody and the affimer framework,[16,17] were generated by selection from phage display libraries. They were found to recognize their targets predominantly in a SIM-like manner and to interfere with SUMO-dependent processes when expressed at high level.

Well-characterized probes for budding yeast SUMO are unavailable. We therefore set out to develop such tools. To enhance our chances of isolating SIM-independent binders that would not interfere with cellular functions, we chose a scaffold based on designed ankyrin repeat proteins (DARPins).[18] These consist of multiple tightly packed ankyrin repeats (ARs) of 33 amino acids each, with randomized residues in the surfaces of α helices and the β turns that connect the AR modules. Jointly, the ARs form a concave, groove-like interaction surface, making them particularly suited to the recognition of native protein surfaces and providing the opportunity for an alternative mode of Smt3 recognition.

Here, we report the isolation and characterization of Smt3-specific DARPins. Among the selected clones, we identified binders with a wide range of affinities and an inhibitory effect on SUMOylation. Structural studies identify the SIM-binding site as a preferred surface for SUMO recognition, albeit via a binding mode distinct from the SUMO-SIM interaction. In addition to these inhibitory DARPins, we identified clones that recognize an alternative surface of Smt3 and show little interference with SUMOylation-dependent processes in cells. In contrast to fluorescently tagged Smt3, the DARPins are applicable in a compartment-specific manner. By employing them in cells, we found that the essential function of Smt3 in budding yeast localizes to the nucleus. In addition, we characterized the nuclear SUMOylation pattern in response to DNA damage. Previously, high levels of DNA damage had been reported to induce SUMOylation of chromatin, mediated by the SUMO-E3 Siz2 and targeted toward homologous recombination (HR) factors at resected stretches of single-stranded (ss) DNA.[19–21] We now report an ssDNA-independent reaction that is induced by sublethal amounts of damage not involving DNA double-strand breaks (DSBs). These results validate the Smt3-specific DARPins as tools for the real-time monitoring of Smt3 activities in live yeast and indicate an unexpected level of complexity of chromatin SUMOylation in the DNA damage response.

RESULTS

DARPins recognize free and conjugated Smt3

DARPins[18] against budding yeast Smt3 were selected from a ribosome display library of $>10^{12}$ clones, using Smt3 with an N-terminal MAH_6 and Twin-Strep tag as bait and four rounds of ribosome display.[22–24] Nineteen positive clones were chosen for further characterization.

Sequence analysis revealed considerable diversity among the selected DARPins, featuring clones with two and three AR modules and only two identical clones, A10 and H10 (Figure 1A). This maintenance of high diversity is typical for ribosome display.[25] Interestingly, a one-amino-acid insertion was enriched in several clones. Some clones may have further diversified during the ribosome display rounds, suggested by a shared C-terminal AR module and/or loss of one repeat (Figure S1A). Notably, none of the selected DARPins contained an identifiable SIM in the randomized regions. All DARPins were purified from *E. coli* in good yield and solubility.

To verify their interaction with Smt3, we performed pull-down assays using either free Smt3 or a C-terminal GFP fusion as bait. An unselected DARPin, E3_5, served as negative control.[26] All selected DARPins except for clone E10 were retained by both Smt3 constructs with comparable efficiency, indicating that none of them was likely to differentiate between free and conjugated Smt3 (Figure 1B). We then tested their ability to interfere with an *in vitro* SUMOylation reaction. As a substrate, we chose budding yeast PCNA, which is modified at two lysine residues, K127 and K164.[27–29] Here, the selected DARPins varied strongly in their properties, ranging from near-complete inhibition to no effect (Figure 1C). Based on these initial results, we chose a panel of six largely monodisperse DARPins (Figure S1B) for in-depth characterization, representing clones with two or three AR modules, diverse sequences, and varying abilities to inhibit PCNA SUMOylation. All clones efficiently depleted Smt3 from a total cell lysate, indicating overall high affinities for their target (Figure 1D). In gel filtration, three selected DARPins (A10, F10, and E11) eluted as a stable complex with Smt3, while the others (C10, G11, and B12) engaged with Smt3 less stably (Figure 1E). Clone E10, which was not retained in the initial pull-down experiment and did not inhibit PCNA SUMOylation, failed to co-elute with Smt3 in this assay, confirming that it did not detectably interact with Smt3. Surface plasmon resonance assays were used to characterize the binding of the six selected DARPins to Smt3. Equilibrium K_D varied between 0.27 nM (A10) and 1.2 μM (C10) (Table 1; Figure S1C). Five of the DARPins discriminated between Smt3 and the human homologs SUMO1 and SUMO2, although C10 exhibited measurable affinity for SUMO1, and E11 weakly bound to SUMO2; G11 bound to Smt3 and SUMO1 with similar affinity, but not to SUMO2 (Table 1; Figure S1D).

Smt3-specific DARPins affect SUMOylation, deSUMOylation, and SIM interaction

Our initial PCNA SUMOylation assays (Figure 1C) suggested variable effects of the DARPins on Smt3 conjugation. To assess how general these were, we examined Ubc9-catalyzed synthesis of unanchored Smt3 chains in the presence of the DARPins. To avoid interference from Ubc9 automodification,[30] a K153R mutant of the E2 was used in all following assays. Analysis of a reaction time course revealed inhibitory effects of all DARPins, correlating to some extent with their affinities, with A10 having the strongest impact, while C10, G11, and B12 afforded only mild inhibition

CellPress
OPEN ACCESS

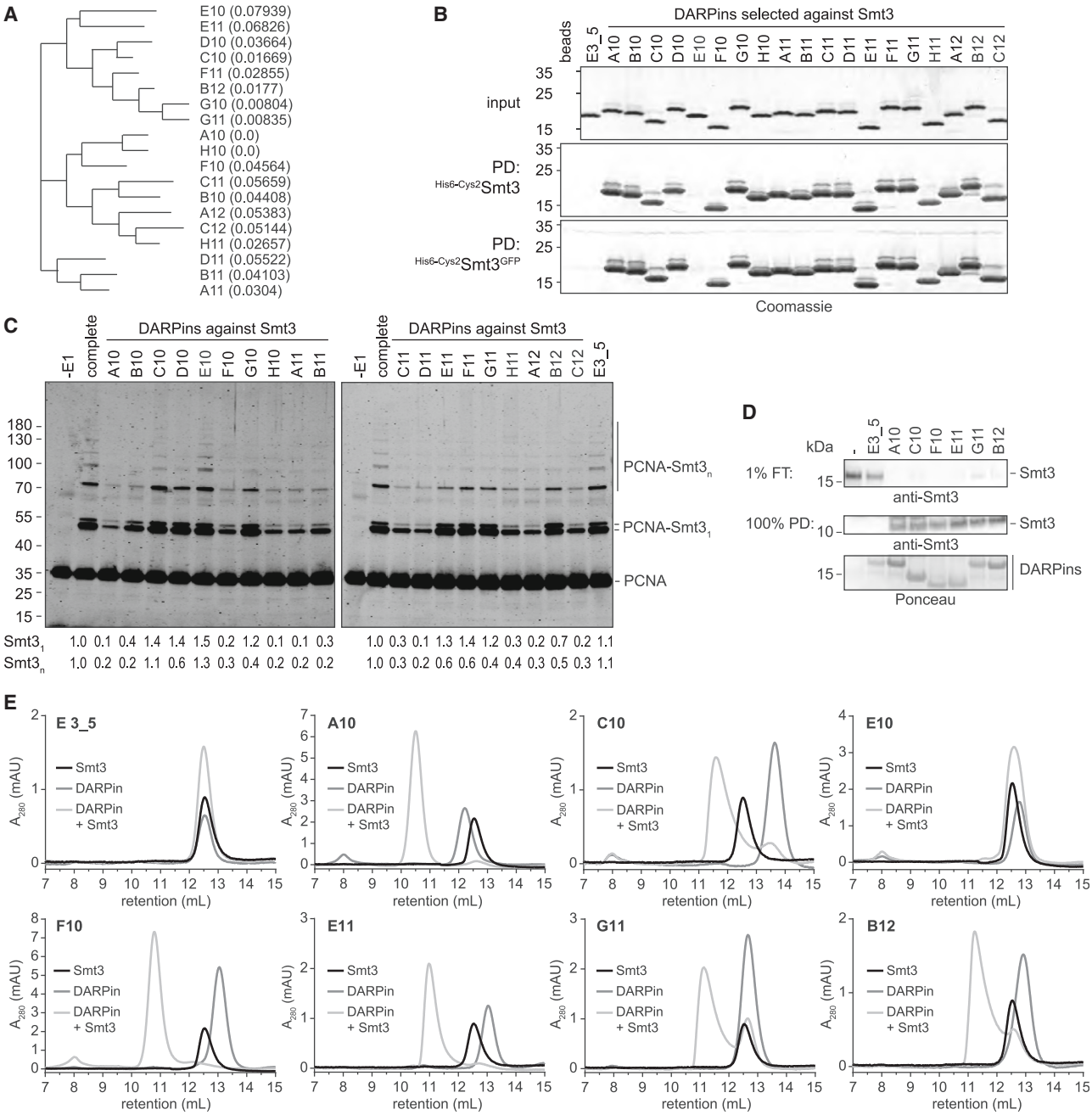

Figure 1. Selected DARPins recognize free and conjugated Smt3

(A) Sequence relations between Smt3-specific DARPins. A neighbor-joining tree, generated from the protein sequences of 19 selected DARPins by multiple alignment, indicating sequence distances. An alignment of amino acid sequences is shown in Figure S1A.

(B) Smt3-specific DARPins do not differentiate between Smt3 bearing a free ($^{His6\text{-}Cys2}$Smt3) or a blocked C terminus ($^{His6\text{-}Cys2}$Smt3^{GFP}). Coomassie-stained gels show retention of DARPins on Smt3-derivatized SulfoLink agarose. DARPin E3_5 serves as a non-selective control (beads, underivatized matrix; PD, pull-down).

(C) Smt3-specific DARPins vary in their ability to inhibit SUMOylation. Western blots showing products of *in vitro* SUMOylation reactions using DNA-loaded recombinant PCNA as substrate in the presence of a 3-fold excess of DARPins over Smt3. Reactions without E1 and without DARPin (complete) served as controls. Note that SUMOylation of PCNA at K127 versus K164 yields products with distinct mobilities.

(D) Selected DARPins deplete Smt3 from yeast extract. Recombinant ^{His8}DARPin^{FLAG} proteins were immobilized on FLAG beads for pull-down assays from total cell lysates, followed by western blot analysis of bound (PD) and unbound (FT) material using antibodies against Smt3.

(E) Smt3-specific DARPins differ in their abilities to form a stable complex with Smt3. Analytical gel filtration profiles (at 280 nm) are shown for equimolar mixtures of selected DARPins with recombinant Smt3 (5 μM each).

Table 1. Affinities and association and dissociation rate constants of Smt3-specific DARPins

	A10	C10	F10	E11	G11	B12
Smt3						
$k_a \pm$ SD (10^5 M^{-1} s^{-1})	8.8 ± 1.1	ND[a]	34.7 ± 18.7	ND[a]	ND[a]	ND[a]
$k_d \pm$ SD (10^{-3} s^{-1})	0.24 ± 0.02	ND[a]	12.6 ± 6.1	ND[a]	ND[a]	ND[a]
$K_D \pm$ SD (nM)	0.27 ± 0.03	1,204 ± 403	3.1 ± 0.7	42.8 ± 6.0	656 ± 15	355 ± 21
hSUMO1						
K_D (nM)	none[b]	2,250[c]	none[b]	none[b]	445 ± 13	none[b]
hSUMO2						
K_D (nM)	none[b]	none[b]	none[b]	>10,000[c]	none[b]	marginal[d]

Standard deviations (SD) were determined from a minimum of three independent measurements unless otherwise noted.
[a]Not determined, as k_d and/or k_a exceeded the dynamic range of the instrument.
[b]No binding detected at up to 6.6 μM DARPin.
[c]Based on a single equilibrium measurement.
[d]Not quantified, no saturation at 20 μM DARPin.

(Figure 2A). The use of an Smt3-specific E3, Siz1,[31] did not change this pattern (Figure S2A). Concentration-dependent inhibition was observed in a fluorescence resonance energy transfer (FRET)-based substrate SUMOylation assay[32,33] using an eCFP-tagged fragment of RanGAP1 (amino acids 400–589) and ^{YFP}Smt3 (Figures 2B and S2B). Again, clone A10 afforded the strongest inhibition at an equimolar ratio. At a 10-fold molar excess, all DARPins strongly impeded RanGAP SUMOylation.

To dissect which step(s) of the SUMOylation cascade the DARPins impeded, we separately monitored thioester formation of Smt3 with the E1 subunit Uba2 and with the E2 Ubc9. Inhibitory effects on E1 thioester formation correlated well with the affinity of the DARPins for Smt3, as A10 was strongly inhibitory, while F10 and E11 exhibited partial effects, and C10, G11, and B12 had virtually no effect (Figures 2C and S2C). Thus, the effects of A10, F10, and E11 on SUMOylation can largely be attributed to their inhibition of Smt3 activation by E1. DARPins that did not inhibit E1 thioester formation had no measurable effect on thioester formation with Ubc9 either (Figure S2D).

Strong interactions with Smt3 should impede not only Smt3 conjugation but also deconjugation. We therefore followed Ulp1-mediated cleavage[34,35] of a linear Smt3-GFP fusion protein as a mimic of an Smt3 conjugate. In these reactions, only clone A10 produced a measurable delay (Figures 2D and S2E).

Finally, we asked whether the DARPins would interfere with the interaction between Smt3 and a conserved SIM. To this end, we performed pull-down assays with biotinylated Smt3 immobilized on streptavidin beads and purified RNF4, a SUMO-dependent ubiquitin E3 that harbors four tandem SIMs and thus exhibits a high avidity for Smt3.[36,37] A 10-fold molar excess of DARPin A10, F10, or B12 over RNF4 largely abolished retention of RNF4, while C10 had an intermediate effect, and E11 and G11 only mildly interfered with RNF4 binding (Figures 2E and S2F). Unlike the inhibitory effects on Smt3 conjugation, interference with the Smt3-SIM interaction did not correlate with the relative affinities of the DARPins. This suggests distinct binding modes and varying degrees of overlap with the SIM-binding site on Smt3.

In summary, our quantitative analysis demonstrates a wide range of affinities of the DARPins for yeast Smt3, spanning more than three orders of magnitude and resulting in variable degrees of interference with SUMOylation *in vitro*, mostly at the level of E1. As a consequence, the high-affinity DARPins inhibit both substrate modification and polymerization of Smt3. In contrast, most of the DARPins do not measurably interfere with deSUMOylation. Notably, the observed differences in the ability to inhibit the Smt3-SIM interaction may reflect the use of distinct interaction surfaces of Smt3 by the DARPins. The individual clones are therefore expected to differ in their ability to interfere with downstream effects of SUMOylation *in vivo*.

Crystal structures of DARPin·Smt3 complexes reveal alternative modes of SUMO recognition

To gain insight into the recognition of Smt3 by the DARPins, we solved the structures of clones A10 and C10, representing a strong and a weak binder, in complex with Smt3 by X-ray crystallography (Table S1). The flexible N terminus (amino acids 1–19) was deleted from Smt3 for this purpose. Structures were solved by molecular replacement with known structures of Smt3[38] (PDB: 1EUV) and DARPin E3_5[26] (PDB: 1MJ0).

The A10 complex crystallized with two nearly identical A10·Smt3 pairs in the asymmetric unit (Figure S3A). The average buried interface of 956 Å^2 amounts to ∼21% of the solvent-accessible surface of Smt3. The cartoon image of the complex (Figure 3A) illustrates that A10 engages with Smt3 via all four of its β turns and covers the surface around the SIM-binding site of Smt3. A close-up view into Smt3's hydrophobic groove (Figure 3B) shows contacts of A10 with Smt3 residues usually involved in SIM binding, such as I35, F37, and L48. On the side of A10, a series of aromatic amino acids within the β turns provides a hydrophobic interaction surface contacting the SIM-binding site, e.g., at I35, but also reaching beyond it and engaging in possible cation-π interactions, such as W83 with R55 in the SIM-binding site of Smt3 and W147 with the adjacent K54 of Smt3 (Figure 3C). The interface also involves polar and charged residues with predicted hydrogen bonds and salt bridges between A10 and Smt3 both within the SIM-interaction site, such as N160-R47, and surrounding it, e.g., D157-R46, Y81-Q56, and W147-E59 (Figures S3B and S3C). In contrast to A10, clone C10 uses only its second and third β turns for binding

CellPress
OPEN ACCESS

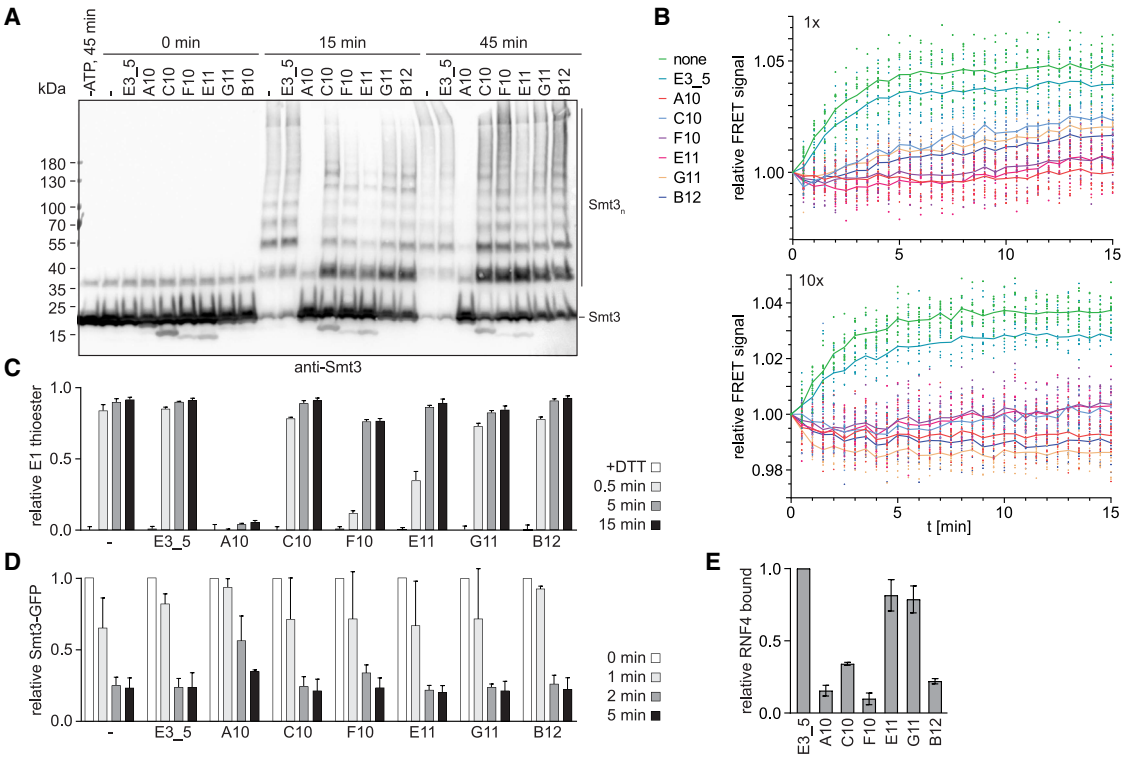

Figure 2. Smt3-specific DARPins affect SUMOylation, deSUMOylation, and SIM interaction

(A) Smt3-specific DARPins inhibit formation of unanchored Smt3 chains to varying degrees. SUMOylation reactions were set up with 1 μM Smt3 and a 5-fold molar excess of DARPins. A time course was analyzed by western blotting against Smt3. Analogous reactions in the presence of Siz1 are shown in Figure S2A.

(B) Smt3-specific DARPins affect *in vitro* substrate SUMOylation. Reactions containing 100 nM eCFP-tagged RanGAP1 (amino acids 400–589) and ^{YFP}Smt3 were set up with an equimolar amount or a 10-fold excess of DARPins in three to five replicates. Conjugation was monitored by FRET. The graphs shows mean values (lines) and individual data points. Western blots of the final products are shown in Figure S2B.

(C) Smt3-specific DARPins inhibit E1 thioester formation to varying degrees. Uba2 thioester formation in the presence of 500 nM Aos1·Uba2, 5 μM Smt3, and a 5-fold molar excess of the indicated DARPins was detected on non-reducing gels and quantified relative to total Uba2 signals (under reducing conditions). Values represent averages and standard deviations of three to six independent assays. Representative gel images are shown in Figure S2C.

(D) Smt3-specific DARPins inhibit Ulp1-mediated deSUMOylation to varying degrees. Cleavage of a linear Smt3-eGFP fusion protein (4 μM) in the presence of a 5-fold molar excess of DARPins was monitored in a gel-based assay. Full-length Smt3-eGFP was quantified relative to the level before addition of Ulp1. Values represent averages and standard deviations of three independent assays. Representative gel images are shown in Figure S2E.

(E) Smt3-specific DARPins interfere with SUMO-SIM interaction to varying degrees. Retention of RNF4 by biotinylated Smt3 immobilized on streptavidin beads was monitored in the presence of a 10-fold molar excess of the indicated DARPins over RNF4 and quantified by western blotting. Values represent averages and standard deviations from three independent experiments. A representative western blot is shown in Figure S2F.

to Smt3 (Figure 3D) and covers only 11% of the modifier's solvent-accessible surface (543 Å^2). In addition to mainly hydrophobic interactions with the SIM-binding groove, e.g., with residues F37, I39, L48, and A51 (Figure 3E), C10 also contacts the adjacent β sheet of Smt3, e.g., at N25 (Figure 3F).

A comparison of the footprints of the DARPins on Smt3 with those of a SIM peptide[39] and a monobody that was previously shown to also interact with the SIM-binding site[16] reveals strong similarities in the surfaces of Smt3 that are recognized by the various molecules (Figure 3G). The larger footprint involved in the interaction with A10 is consistent with the highest affinity of this clone. Interestingly, however, while the monobody occupies the SIM-binding groove in exactly the same manner as the SIM peptide, employing aromatic residues in place of the hydrophobic aliphatic amino acids characteristic of the SIM consensus, neither A10 nor C10 forms an intermolecular β sheet with Smt3, and C10 clearly touches residues outside the SIM interaction site.

To further explore the interaction mode of A10 with Smt3, we determined its affinities for a series of Smt3 mutants (Table 2; Figure S3D). Considering the placement of R47 in a polar environment at the interface (Figure S3C), we mutated this residue to alanine. Surprisingly, this enhanced the affinity for A10 nearly 5-fold to ~60 pM, suggesting that the removal of steric bulk at this site improves binding. To assess the contributions of hydrophobic interactions to A10 binding, we mutated three bulky residues within the SIM-binding site (I35, F36, and F37) to aspartic acid (Smt3^{3D}). These mutations afforded only a moderate reduction in affinity of about 7-fold, indicating that the hydrophobic nature of the SIM-binding groove is not essential for recognition by A10. A more severe loss of affinity (~17-fold) was observed when a set of acidic residues (E34, E50, and E59) surrounding the SIM-binding site (Figure S3E) was mutated to alanine (Smt3^{3A}), suggesting that charged or polar interactions outside the hydrophobic groove are more important for A10 binding than the hydrophobic contacts

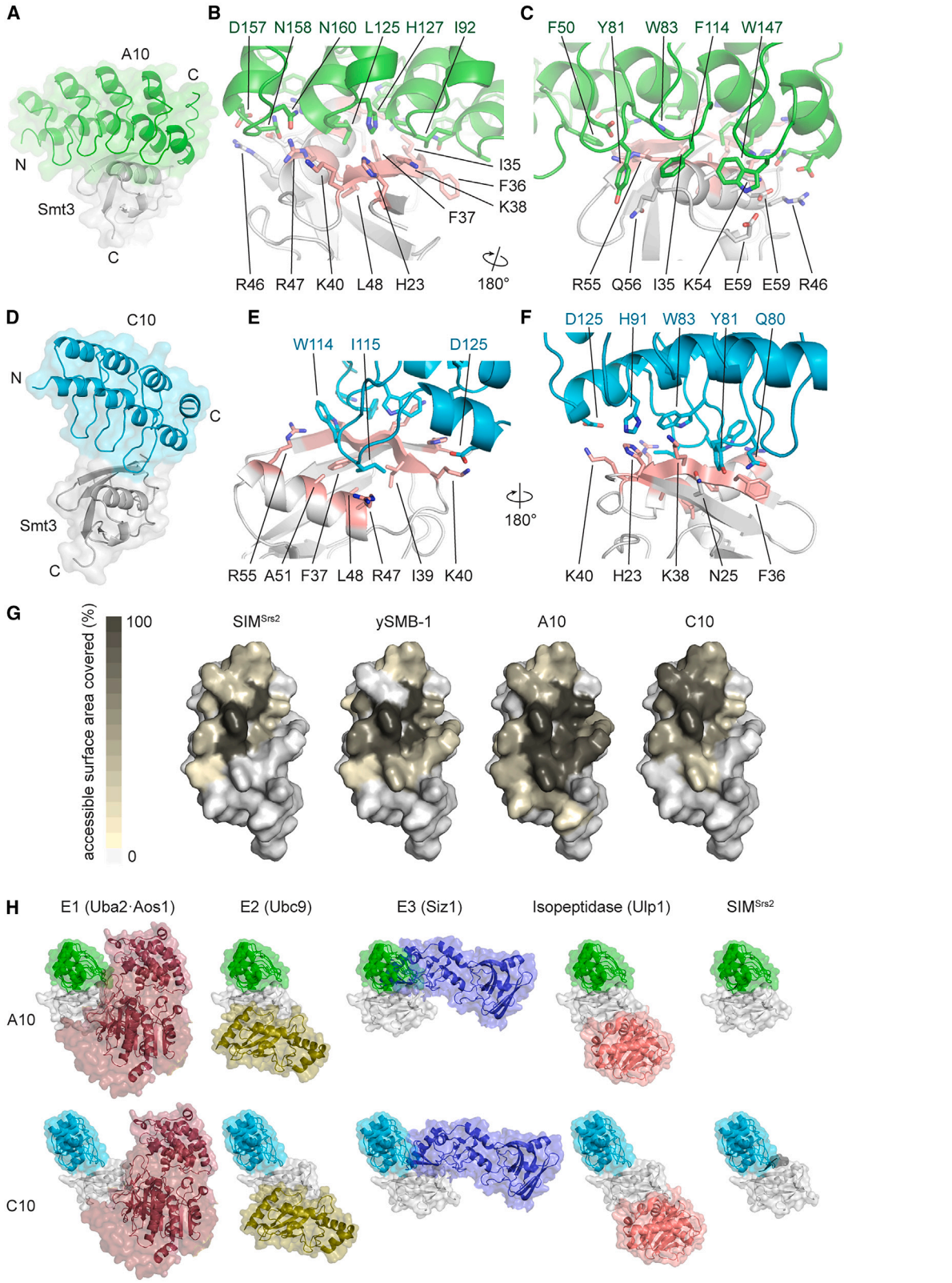

(legend on next page)

Table 2. Affinities and association and dissociation rate constants of DARPins A10 and C10 for selected Smt3 mutants

	A10								C10		
Smt3	WT	R47A	3D	3A	3X	5X	11X	SIMX	WT	11X	SIMX
$k_a \pm$ SD (10^5 M^{-1} s^{-1})	8.8 ± 1.2	12.4 ± 5.7	9.4 ± 7.1	2.1 ± 0.6	2.5 ± 0.9	3.7 ± 1.3	none[a]	none[b]	ND[d]	ND[d]	ND[d]
$k_d \pm$ SD (10^{-3} s^{-1})	0.24 ± 0.02	0.08 ± 0.04	1.1 ± 0.9	0.9 ± 0.4	7.6 ± 0.7	43.9 ± 34.8	none[a]	none[b]	ND[d]	ND[d]	ND[d]
$K_D \pm$ SD (nM)	0.27 ± 0.03	0.06 ± 0.01	1.9 ± 1.5	4.5 ± 1.6	25.2 ± 2.8	110 ± 52	none[a]	none[b]	1,204 ± 403	63.2 ± 31.9	none[c]
Fold change in K_D	1×	0.2×	7×	17×	93×	407×	–	–	1×	0.05×	–

Standard deviations (SD) were determined from a minimum of three independent measurements. Note that some fits (Figure S3D) may suffer from bulk effects. Smt3 mutants are abbreviated as 3D (I35D, F36D, F37D), 3A (E34A, E50A, E59A), 3X (F36H, R47K, E59P), 5X (K41M, R46K, K54Q, K58V, E59P), 11X (H23Y, N25K, F36H, I39V, K41M, R46K, R47K, A51S, K54Q, K58V, E59P), and SIMX (T22A, I35S, F37S, K38E, K40E, T43A, L48S, R55E, N86A). WT, wild type.
[a]No binding detected at up to 2.2 μM DARPin.
[b]No binding detected at up to 6.6 μM DARPin.
[c]No binding detected at up to 20 μM DARPin.
[d]Not determined, as k_d and/or k_a exceeded the dynamic range of the instrument.

with the groove. We then successively exchanged interface residues in Smt3 with their equivalents in human SUMO1, based on the argument that SUMO1 shares more similarity with Smt3 than SUMO2 but does not measurably interact with A10. As expected, these mutations ($Smt3^{3X}$, F36H, R47K, and E59P; $Smt3^{5X}$, K41M, R46K, K54Q, K58V, and E59P; and $Smt3^{11X}$, H23Y, N25K, F36H, I39V, K41M, R46K, R47K, A51S, K54Q, K58V, and E59P) caused dramatic reductions in affinity. Binding was also abolished by a non-overlapping set of mutations affecting the SIM-binding patch ($Smt3^{SIMX}$, T22A, I35S, F37S, K38E, K40E, T43A, L48S, R55E, and N86A).

$Smt3^{11X}$ and $Smt3^{SIMX}$, featuring exchange of interface residues specific for human SUMO1 and for SIM binding, respectively, were also assayed for their interactions with clone C10 (Table 2; Figure S3F). $Smt3^{11X}$ exhibited a 20-fold enhanced affinity for C10, consistent with the cross-reactivity of C10 toward SUMO1. In contrast, no interaction was detected between C10 and $Smt3^{SIMX}$, confirming the importance of the hydrophobic SIM-interaction patch for Smt3 recognition by C10.

Taken together, these results support our structural data suggesting that A10 and C10 recognize a surface of Smt3 that is centered on the hydrophobic groove of the SIM-binding site but do not align with the β sheet of SUMO. Binding by A10 is additionally supported by polar or charged interactions surrounding the hydrophobic groove.

The X-ray structures also explain the properties of the DARPins with respect to our *in vitro* SUMOylation and deSUMOylation assays (Figure 3H). Superpositions of the DARPin·Smt3 structures and Smt3 in complex with components of the yeast SUMO system[34,39–42] reveal clashes of the DARPins not only with the SIM peptide but also with the E3 Siz1. A10 also clashes with E1, whereas E2 and the isopeptidase (Ulp1) occupy non-overlapping surfaces of Smt3. These geometries confirm our finding that the effect of A10 is mostly due to an interference with E1 thioester formation, while C10 does not affect the activities of the core SUMOylation factors E1 and E2.

DARPins locate the essential function of Smt3 in the nucleus

Strong interactions of the DARPins with Smt3 should interfere with the essential function of the modifier in cells. To test this prediction, we expressed selected DARPins in yeast as C-terminal GFP fusions under control of a doxycycline-inducible *Tet* promoter.[43] In contrast to the non-selective clone, E3_5,

Figure 3. Crystal structures of DARPin·Smt3 complexes reveal alternative modes of Smt3 recognition
(A) DARPin A10 binds to the SIM-binding surface of Smt3. N and C termini of A10 (green) and Smt3 (gray) are indicated in the cartoon and surface model of the A10·Smt3 complex.
(B) A detailed view of the A10·Smt3 interface illustrates interactions at the hydrophobic cleft between the Smt3 α helix and β sheet. Residues involved in SIM binding are colored in pink.
(C) A series of aromatic residues within the four β turns of DARPin A10 contacts the Smt3 surface. The image is rotated by 180° relative to the one in (B).
(D) DARPin C10 binds to the SIM-binding surface of Smt3. N and C termini of C10 (cyan) and Smt3 (gray) are indicated in the cartoon and surface model of the C10·Smt3 complex.
(E) A detailed view of the C10·Smt3 interface illustrates interactions at the hydrophobic cleft between the Smt3 α helix and β sheet. Residues involved in SIM binding are colored in pink.
(F) C10 uses its second and third β turn to engage with additional residues of the Smt3 β sheet. The image is rotated by 180° relative to the one in (E).
(G) Footprints of Smt3-binding proteins reveal a preference for Smt3's SIM-binding region. A surface model of Smt3 (PDB: 1L2N, C terminus pointing downward) was colored according to the percentage of accessible surface area buried in the interface with the indicated proteins: a SIM peptide from budding yeast Srs2 (PDB: 3V62), the Smt3-specific monobody ySMB-1 (PDB: 3QHT), A10, and C10.
(H) Alignment of DARPin·Smt3 complexes (Smt3, gray; A10, green; C10, cyan) with structures of Smt3 in complex with components of the SUMO system illustrates relevant interaction surfaces: Uba2·Aos1 (PDB: 1Y8R), Ubc9 (PDB: 2EKE), Siz1 (PDB: 5JNE), Ulp1 (PDB: 1EUV), and SIM^{Srs2} (PDB: 3V62). Smt3's C terminus points to the right.

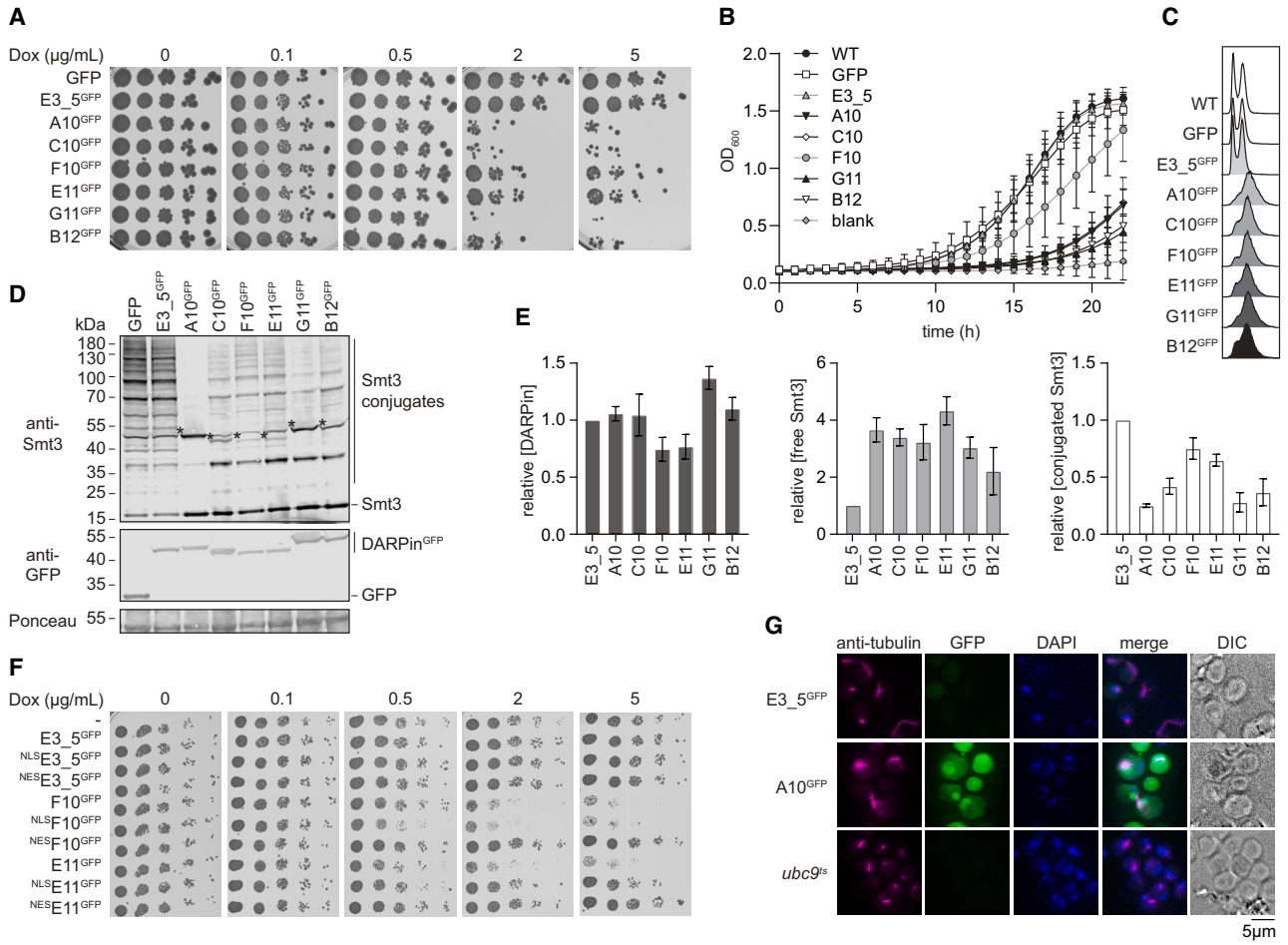

Figure 4. DARPins locate the essential function of Smt3 in the nucleus

(A) Smt3-specific DARPins interfere with growth on solid medium. Yeast strains expressing the indicated GFP-tagged DARPins under control of the *Tet*-promoter were spotted in serial dilutions onto SC-complete plates containing the indicated concentrations of doxycycline (Dox). Growth was recorded after 3 days.

(B) Smt3-specific DARPins interfere with growth in liquid culture. Optical densities (OD_{600}) of exponential cultures were recorded after induction of $DARPin^{GFP}$ expression with 2 µg/mL doxycycline. Values represent mean and standard deviations from three replicates per data point.

(C) Smt3-specific DARPins cause a cell-cycle arrest. Flow cytometry profiles were recorded after induction of $DARPin^{GFP}$ expression with 2 µg/mL doxycycline for 20 h.

(D) Smt3-specific DARPins interfere with SUMOylation *in vivo*. Free and conjugated Smt3 as well as $DARPin^{GFP}$ proteins were monitored by western blotting of total lysates of cells after $DARPin^{GFP}$ expression with 2 µg/mL doxycycline for 20 h. Ponceau S staining served as loading control. Bands marked with asterisks correspond to reactivity of the anti-Smt3 antibody with Smt3 trapped by the DARPins on the membrane (see Figure S4E). They were excluded from quantification.

(E) Expression of Smt3-specific DARPins causes accumulation of free Smt3 and depletion of Smt3 conjugates. Western blot signals were quantified from experiments performed as in (D). Cross-reacting signals of the DARPins on anti-Smt3 blots (see Figure S4E) were subtracted from the signals of Smt3 conjugates. Values represent mean and standard deviations from three independent experiments.

(F) Smt3-specific DARPins exert their inhibitory effect in the nucleus. Growth on indicated concentrations of doxycycline was recorded for strains harboring DARPins $F10^{GFP}$ or $E11^{GFP}$ fused to a nuclear localization signal (NLS) or nuclear export signal (NES). A control blot is shown in Figure S4G.

(G) Expression of DARPin $A10^{GFP}$ (2 µg/mL doxycycline for 4 h) causes a G2/M cell-cycle arrest comparable to *ubc9*^{ts} at the restrictive temperature. Strains were grown at 37°C. Tubulin was detected by immunofluorescence in fixed cells; $DARPin^{GFP}$ proteins were detected via GFP fluorescence; nuclei were stained by DAPI (DIC, differential interference contrast).

Smt3-specific DARPins were enriched in the nucleus (Figures S4A and S4B). Co-localization with ^{mCherry}Smt3 confirmed that this reflects the distribution of Smt3 itself, indicating that the DARPins recognize their target in cells (Figures S4C and S4D). At high expression levels, all DARPins inhibited growth to some extent (Figures 4A and 4B) and caused an accumulation of cells in the G2/M phase of the cell cycle (Figure 4C). These effects correlated more with the expression levels of the DARPins than with their affinity or their interference with the Smt3-SIM interaction (Figure 4A). Consistent with the *in vitro* results, expression of the DARPins reduced the amount of Smt3 conjugates in cells and increased the level of free Smt3 (Figures 4D, 4E, and S4E), confirming the inhibitory action on SUMOylation. DARPins F10 and E11, which exhibited the mildest effects on growth and Smt3 conjugation, were also expressed to a somewhat lower level than the other DARPins in these assays

CellPress
OPEN ACCESS

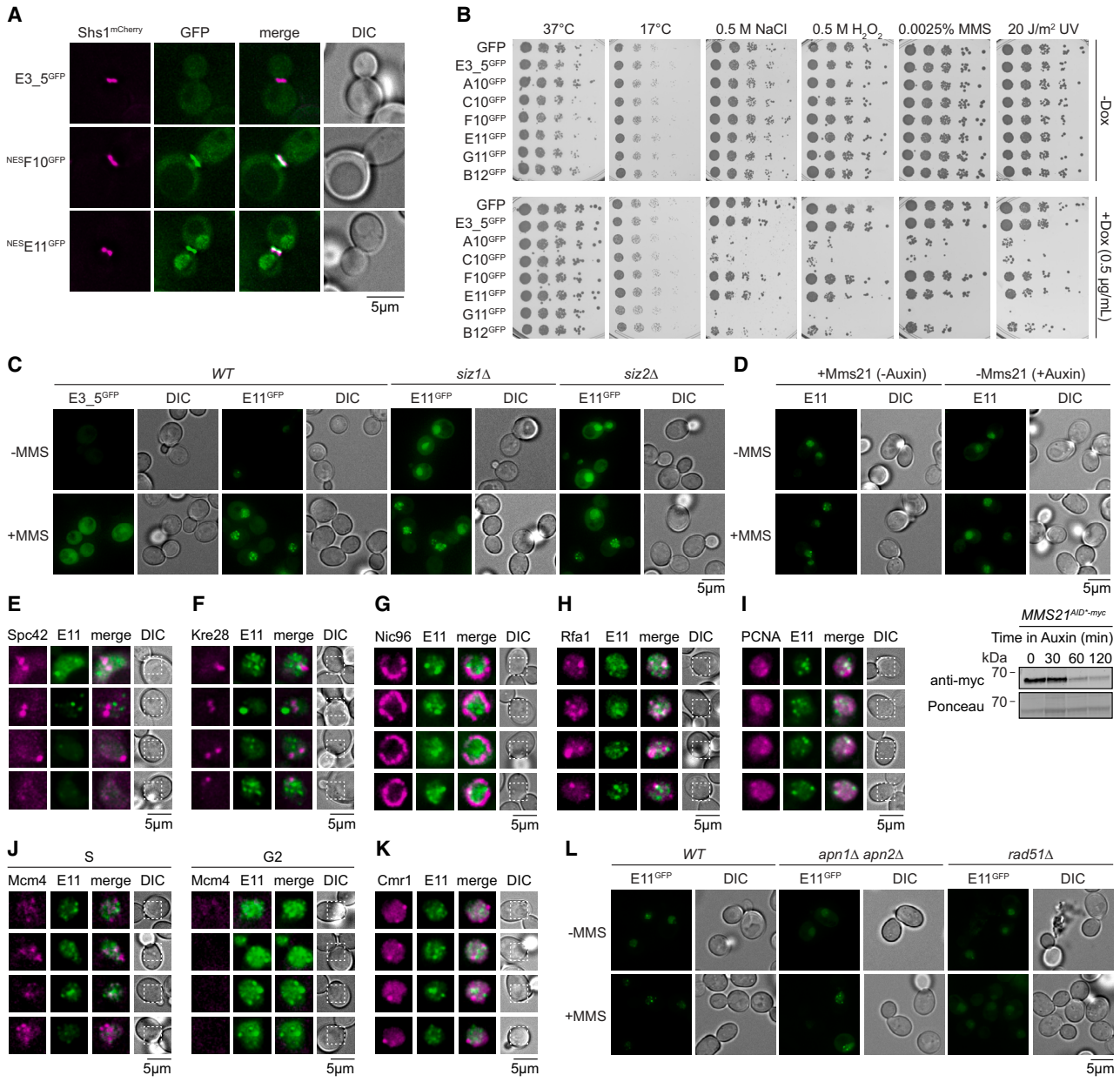

Figure 5. Smt3-specific DARPins can report on compartment-specific SUMOylation events

(A) NES-tagged DARPins track the SUMOylation of mitotic septins. Fluorescence images show G2/M cells harboring Shs1^{mCherry} and the indicated GFP-tagged DARPins after induction of DARPin expression with 0.5 μg/mL doxycycline for 20 h.

(B) Expression of Smt3-selective DARPins sensitizes yeast toward osmotic, oxidative, and genotoxic stress, but not toward heat or cold stress. Cells harboring DARPin expression constructs were spotted onto plates with or without 0.5 g/mL doxycycline. Where indicated, plates contained NaCl, H_2O_2, or MMS. Alternatively, they were exposed to 20 J/m^2 UV irradiation before incubation or incubated at the indicated temperature during the growth period. Colony formation was recorded after 3 days.

(C) MMS causes accumulation of Smt3 in nuclear foci independent of Siz1 or Siz2. Fluorescence images are shown after induction of wild-type (WT) or the indicated mutant DARPins with 0.5 μg/mL doxycycline for 20 h. Where indicated, cells were treated with 0.02% MMS for 90 min.

(D) Accumulation of MMS-induced Smt3 foci depends on Mms21. Top: fluorescence images were obtained as in (C), using a strain expressing E11^{GFP} and harboring a degron-tagged *MMS21* allele. Degradation of Mms21^{AID*myc} was induced with 1 mM auxin prior to treatment with 0.02% MMS for 90 min. Bottom: western blot showing protein levels of Mms21^{AID*myc}. Ponceau S staining served as loading control.

(E–K) MMS-induced Smt3 foci exhibit little or no co-localization with various subnuclear features. Induction of E11^{GFP} expression, MMS treatment, and fluorescence microscopy were performed as in (C) in strains harboring an mCherry- or mRuby2-tagged marker protein to indicate (E) spindle pole body (Spc42^{mCherry}), (F) kinetochore (Kre28^{mCherry}), (G) nuclear pore complex (Nic96^{mCherry}), (H) ssDNA (Rfa1^{mRuby2}), (I) PCNA (^{mRuby2}Pol30), (J) replicative helicase

(legend continued on next page)

(Figure 4E). In fact, inhibition of SUMOylation correlated with doxycycline concentration for both the strongly inhibitory A10 and the mildly inhibitory E11 (Figure S4F).

The G2/M arrest of yeast expressing the Smt3-specific DARPins was reminiscent of temperature-sensitive *ubc9*^{ts} mutants.[14] This suggested that the DARPins could be used to explore the nature of the essential function of Smt3. We therefore asked in which cellular compartment the DARPins exerted their toxic effect. To this end, we expressed two mildly inhibiting DARPins, F10 and E11, with either a nuclear localization signal (NLS) or a nuclear export signal (NES). We found that both DARPins inhibited growth only when fused to an NLS or without any localization signal, but not when largely forced into the cytoplasm by means of an NES (Figures 4F and S4G). Immunofluorescence of cells expressing the strongly inhibitory clone A10 confirmed that the DARPin caused a cell-cycle arrest before anaphase, i.e., with short spindles, comparable to *ubc9*^{ts} cells at non-permissive temperature (Figure 4G).

Thus, the DARPins can be used as effective inhibitors of Smt3 conjugation in cells at high expression levels, and they interfere with the essential function of the modifier in the nuclear compartment.

DARPins act as compartment-specific SUMOylation reporters

Low-level expression of the DARPins, in particular clones F10 and E11, did not compromise growth. These DARPins might therefore serve as *in vivo* SUMOylation reporters. As a proof-of-principle experiment, we expressed GFP- and NES-tagged F10 and E11 in a strain harboring an mCherry-tagged septin, Shs1, using a low doxycycline concentration. Consistent with septin SUMOylation in mitosis,[44] we observed a co-localization of the DARPins with the mCherry signal at the bud neck in large-budded cells (Figure 5A). This indicates that fluorescent NES-tagged DARPins can be used to follow cytoplasmic SUMOylation events without interference from the large nuclear pool of Smt3 in live yeast.

Expression of DARPins at subtoxic levels might also be used to sensitize cells specifically to stress conditions under which SUMOylation is important. To explore this, we expressed the DARPins at low doxycycline concentration (0.5 μg/mL), where none of them interfered with growth (Figure 4A), and exposed cells to heat stress, cold stress, osmotic stress, oxidative stress, or DNA damage (Figure 5B). While the DARPins did not affect the cells' reaction to heat or cold stress, DARPins A10, C10, and G11 strongly sensitized cells to osmotic, salt, and genotoxic stress. Thus, Smt3-specific DARPins can serve to investigate the functions of SUMOylation in specific cellular pathways by selectively sensitizing cells toward relevant stress conditions.

DARPins reveal DNA-damage-induced chromatin SUMOylation

To explore the contributions of SUMOylation to genome maintenance, we chose DARPin E11 as a reporter because this clone neither competed with the SUMO-SIM interaction nor interfered with growth or sensitized cells toward DNA damage at moderate expression levels. In addition, its interaction was unaffected by removal of SUMO's N terminus (Figure S5A); thus, SUMO chain formation was deemed unlikely to affect detection by this DARPin.

Upon treatment with the alkylating agent methyl methanesulfonate (MMS), we detected accumulation of E11^{GFP} in nuclear foci (Figure 5C). Co-localization with ^{mCherry}Smt3 confirmed that they represented SUMO (Figure S5B). Foci were also detected after treatment with agents causing bulky adducts, such as 4-nitroquinolin oxide (4-NQO) and ultraviolet (UV) irradiation, but not after ribonucleotide depletion by hydroxyurea (HU) treatment (Figure S5C), after induction of DSBs via expression of an endonuclease, *Asc*I (Figure S5D), or in response to proteotoxic stress induced by a proteasome inhibitor, MG132 (Figure S5E). Chromatin spreads confirmed association of the foci with chromatin (Figure S5F), suggesting that they represented sites of DNA damage. To identify possible underlying Smt3 substrates, we tested abundant Smt3 targets involved in DNA replication and/or repair such as PCNA,[27] the ssDNA-binding replication protein A (RPA) complex,[45] and the topoisomerases Top1[46] and Top2.[47] However, mutating major SUMOylation sites on PCNA or the RPA subunit Rfa1, deletion of Top1, or auxin-mediated depletion of the essential Top2 protein did not diminish MMS-induced E11^{GFP} foci (Figures S5G–S5J).

It therefore appeared possible that the MMS-induced foci were not caused by a single dominant substrate but instead reflected damage-associated group modification of chromatin. Previously, this phenomenon had been observed in response to high doses of MMS (0.2%–0.3%) or UV radiation (80–150 J/m^2) and was attributed to modification of a diverse set of DNA replication and repair proteins associated with various pathways, including HR and nucleotide (NER) and base excision repair (BER).[20,21,48] According to these reports, SUMOylation is mediated by the SUMO-E3 Siz2[21] or a combination of Siz2 and the related E3, Siz1.[48] However, deletion of *SIZ1* and/or *SIZ2* did not abolish the formation of damage-induced SUMO foci (Figures 5C and S5C). Instead, we found the essential SUMO-E3, Mms21, and its catalytic activity to be required (Figures 5D and S5K). Accordingly, mCherry-tagged Mms21 partially overlapped with DARPin E11^{GFP} (Figure S5L).

As SUMOylation had been implicated in the relocalization of persistent DSBs to nuclear pores,[49–51] we systematically tested whether MMS-induced foci were associated with particular subnuclear features. Based on the characteristic crescent shape of the yeast nucleolus, we excluded this subcompartment as a preferred site of Smt3 foci. As expected from their damage dependence, neither spindle pole bodies (Spc42^{mCherry}) nor kinetochores (Kre28^{mCherry}) overlapped with E11^{GFP} (Figures 5E and 5F), even though Kre28 is a known target of Smt3.[52] Notably, we did not detect any co-localization with a nuclear pore component, Nic96^{mCherry}, either (Figure 5G).

(Mcm4^{mCherry}), and (K) INQ (Cmr1^{mCherry}). Images show individual nuclei from areas highlighted in the corresponding DIC images. In (J), the left and right groups of images show S- and G2-phase cells, respectively, selected by MCM localization and bud size.
(L) MMS-induced Smt3 foci arise independent of BER, but are dependent on HR. Induction of E11^{GFP} expression, MMS treatment, and fluorescence microscopy were performed as in (C).

Siz2-mediated group SUMOylation is triggered by exposed ssDNA arising from the resection of DSBs.[19,21] In the absence of DSBs, ssDNA that could trigger SUMOylation, but not necessarily relocalization to the nuclear pore, also emerges at stalled replication forks,[53] in postreplicative daughter-strand gaps,[54] or at NER intermediates.[55] However, we observed little correlation of the E11^{GFP} signal with Rfa1^{mRuby2} (Figure 5H), again suggesting that the SUMOylation pattern upon exposure to a non-lethal dose of MMS (0.02%) differs from the previously reported Siz2-dependent response in that it does not overlap with extended stretches of ssDNA. Association with stalled or active replication forks was excluded by a lack of strong co-localization with ^{mRuby2}PCNA or a subunit of the replicative helicase, Mcm4^{mRuby2} (Figures 5I and 5J). The latter experiment demonstrated that MMS-induced foci were not limited to S phase, but also appeared in G2, where the MCM complex localizes to the cytoplasm. No preferential co-localization of E11^{GFP} was found with the intranuclear quality control compartment (INQ; marked by Cmr1^{mCherry}), a reservoir of various repair factors, including the SUMO-targeted ubiquitin ligase Slx5-Slx8[56] (Figure 5K). Finally, we examined whether the foci were associated with specific DNA repair pathways, such as BER or HR (Figure 5L). In an *apn1Δ apn2Δ* mutant, MMS-induced foci still accumulated, arguing against their involvement in BER. In contrast, foci were absent in *rad51Δ*, suggesting that they emerge as a result of HR.

Taken together, application of a GFP-tagged DARPin as an Smt3-specific biosensor demonstrates Mms21- and Rad51-dependent, chromatin-associated SUMOylation in response to sublethal doses of DNA damage. The underlying process clearly differs from the group SUMOylation involving HR factors that is observable upon massive induction of DSBs.

DISCUSSION

Insight into the molecular recognition of SUMO

The DARPin framework has allowed us to isolate Smt3 binders with interaction modes that differ remarkably from other SUMO-specific probes and receptors. Gilbreth et al. used the fibronectin type III domain as a scaffold for so-called monobodies, where three randomized loops mimic the complementarity-determining regions of immunoglobulins.[16] Following initial selections against yeast Smt3 and library redesign, probes with good paralog specificity and K_D values below 100 nM were obtained and validated for human SUMO1 and SUMO2/3. Structural studies of one yeast-specific clone implied that these monobodies recognize the SIM-binding site of SUMO via a peptide loop aligning with Smt3's SIM-binding groove in a SIM-like fashion. A different scaffold with two variable loops was used by Hughes et al. and yielded paralog-specific as well as non-selective affimers with K_D values between 35 and ~400 nM.[17] Again, a subset of these contained SIM-like sequences in one of their recognition loops, and structural studies confirmed a SUMO-SIM-like interaction mode.[17]

In contrast, DARPins recognize their targets via a concave binding surface composed of multiple short loops and surface residues along the DARPin helices. Intriguingly, the majority of characterized Smt3-specific clones, including A10 and C10, also interfered with SIM binding, suggesting that this face of Smt3 is prone to engaging in protein-protein interactions. However, the binding surface of the DARPin scaffold employed alternative contacts not involving β sheet formation with Smt3. In addition, competition assays indicate that at least two of the DARPins, E11 and G11, recognize a different surface of Smt3 with K_D values below 100 nM. Our strategy to generate probes that would not inhibit *in vivo* functions of SUMOylation by avoiding the selection of SIM-like loops has therefore been successful.

Tools for investigating the budding yeast SUMO system

The wide spectrum of affinities and inhibitory qualities among the selected DARPins offers a range of properties matching relevant applications. All DARPins recognize free as well as conjugated Smt3 and are capable of depleting the modifier from total cell extracts, indicating that the recombinant proteins can act as substitutes for antibodies to identify Smt3 targets by affinity-based isolation and mass spectrometry. When expressed in cells, a subnanomolar binder such as A10 can serve as an inducible inhibitor of cellular SUMOylation that—unlike the *ubc9^{ts}* mutant—does not require a temperature shift and can be tuned in its potency via its expression levels. Addition of a nuclear import or export signal even allows for compartment-specific activity. In this manner, we showed that DARPins inhibit proliferation only when present in the nucleus and not in the cytoplasm. This is consistent with the hypothesis that Smt3's essential function is linked to the activity of the anaphase-promoting complex (APC/C), a large ubiquitin-E3 responsible for inducing the degradation of cell-cycle-relevant nuclear substrates such as the anaphase inhibitor Pds1 and the mitotic cyclins.[57]

At moderate expression levels, none of the DARPins interfered with proliferation. However, a group of clones (A10, C10, and G11) sensitized the host strain to a range of stress conditions, including osmotic, oxidative, and genotoxic stress. We therefore expect that these DARPins can serve as tools to elucidate the contribution of SUMOylation to the relevant cellular pathways.

Finally, another subgroup of selected DARPins, comprising clones E11 and G11, did not compete for SIM binding of Smt3. They are thus unlikely to impede the downstream effects of SUMOylation. Therefore, we validated E11 as an *in vivo* biosensor. When equipped with an NES, it localized to the bud necks of mitotic cells, thus tracing SUMOylation of the mitotic septins[44] without interference from the dominant nuclear Smt3 signal. When not excluded from the nucleus, the most prominent SUMOylation signal detected by E11 was the formation of DNA-damage-induced nuclear foci. Analysis of their origins and properties has now revealed insight into a defined mode of chromatin-associated SUMOylation.

An ssDNA-independent, HR-associated chromatin SUMOylation pathway

Group SUMOylation, i.e., the multisite modification of several proteins acting in the same complex or pathway, has been reported in various cellular processes, including budding yeast septin disassembly,[31,44] ribosome biogenesis,[58] and genome maintenance.[3,59] In response to lethal doses of MMS, yeast cells SUMOylate factors involved in various repair pathways, including HR and non-homologous end joining (NHEJ), BER,

NER, and mismatch repair, and in DNA replication.[20,21,48] However, high concentrations of MMS likely induce a variety of (secondary) lesions in addition to base alkylation, such as single- and double-strand breaks and stalled or collapsed replication forks. These harsh conditions might therefore activate multiple different pathways simultaneously. Indeed, lower MMS doses do not induce the SUMOylation of DSB repair factors.[20] SUMOylation of core HR factors requires Exo1 and is mediated by Siz2,[21] which acts at junctions between single- and double-stranded DNA.[19] These conditions are consistent with activation during DSB resection, but also at postreplicative daughter-strand gaps. In contrast, UV irradiation mainly induces modification of NER proteins in a Siz1- and Siz2-dependent manner.[21,48] We now observed Rad51-dependent, chromatin-associated SUMOylation induced by tolerable doses of MMS, dependent on Mms21 and unrelated to sites of ssDNA, despite the notion that the treatment induces daughter-strand gaps in replicating cells.[54] Moreover, foci were not associated with replication intermediates or any specific subnuclear features. We therefore propose that the relevant SUMOylation targets may represent late recombination intermediates resulting from replicative processing of DNA lesions via sister chromatid exchange. Such a scenario is consistent with Mms21 acting as part of the Smc5/6 complex in preventing gross chromosomal rearrangements and spontaneous DSBs.[60,61] Specifically, Mms21 promotes the dissolution of joint molecules by SUMOylation of the Sgs1-Top3-Rmi1 complex under very similar damage conditions.[62] This model also explains the absence of abundant ssDNA at sites of SUMOylation and the failure of clean DSBs to induce the response.

Limitations of the study

At present, we cannot exclude a single or a small, defined set of unidentified substrates as the origin of damage-induced SUMOylation. Nonetheless, having ruled out major cellular Smt3 targets and identified the responsible E3, we consider it likely that the foci arise by group SUMOylation involving the Sgs1-Top3-Rmi1 complex. Investigating group SUMOylation is often complicated by the redundancy of individual modification events, which cannot easily be abolished by mutating relevant attachment sites. In this situation, Smt3-specific DARPins may prove to be valuable analytical tools to visualize or isolate SUMOylation at defined cellular structures in a substrate-unbiased way. A caveat to this approach is the possibility that the DARPins could prevent efficient SUMOylation or promote unphysiological accumulation of SUMOylated targets by interfering with downstream events, for example, by blocking the binding of an effector protein. Although this is unlikely in the case of E11, given its *in vitro* properties, future studies will need to determine whether the kinetics of dissolution of joint molecules or the rate of damage-induced sister chromatid exchange is affected by the DARPin. Likewise, it will be interesting to explore whether E11^{GFP} can serve for monitoring SUMOylation in other biological contexts. Finally, structural insight into those DARPins that do not interfere with SIM binding will be important to understand their basis of SUMO recognition and to exclude potential bias toward or against SUMO conjugates of more complex topology.

RESOURCE AVAILABILITY

Lead contact

Requests for further information and resources should be directed to and will be fulfilled by the lead contact, Helle D. Ulrich (h.ulrich@imb-mainz.de).

Materials availability

All unique/stable reagents generated in this study are available from the lead contact with a completed materials transfer agreement.

Data and code availability

- The atomic coordinates of the A10·Smt3 and C10·Smt3 complexes have been deposited in the Protein Data Bank, www.rcsb.org, with PDB codes 9G8I and 9GAU, respectively, and are publicly available.
- This paper does not report original code.
- Any additional information required to reanalyze the data reported in this paper is available from the lead contact upon request.

ACKNOWLEDGMENTS

The authors would like to thank IMB's Core Facilities for Flow Cytometry, Microscopy, and Protein Production as well as the Media Lab for their services and Ron Hay, Frauke Melchior, Peter Stirling, Lorraine Symington, Hanna Windecker, and Xiaolan Zhao for plasmids or strains. We thank the staff at the SLS and Dr. Andreas Krämer for help with synchrotron data collection and Birgit Dreier for coordinating the latter part of the DARPin selection project. This research was funded by the Deutsche Forschungsgemeinschaft (DFG, German Research Foundation) – Project-ID 393547839 – SFB 1361 and Project-ID 407023052 – GRK2526/1. The DARPin selection was in part supported by the University of Zurich.

AUTHOR CONTRIBUTIONS

Conceptualization, V.T., R.P.W., and H.D.U.; methodology and investigation, V.T., R.P.W., A.B., C.R., M.M.M., K.E.-O., J.M., T.R., S.F., and J.V.S.; formal analysis, A.B., B.C., and E.W.; writing – original draft, V.T. and H.D.U.; writing – review & editing, R.P.W., C.R., M.M.M., A.P., E.W., and H.D.U.; supervision, project administration, and funding acquisition, A.P., E.W., and H.D.U.

DECLARATION OF INTERESTS

The authors declare no competing interests.

STAR★METHODS

Detailed methods are provided in the online version of this paper and include the following:

- KEY RESOURCES TABLE
- EXPERIMENTAL MODEL AND STUDY PARTICIPANTS DETAILS
- METHOD DETAILS
  - Construction of plasmids
  - DARPin selection and initial screening
  - Preparation of recombinant proteins
  - Sequence analysis
  - *In vitro* interaction assays
  - *In vitro* SUMOylation and deSUMOylation assays
  - *In vitro* thioester assays
  - Crystallization of DARPin·SMT3 complexes
  - Data collection, structure determination, and refinement
  - Manipulation of budding yeast
- QUANTIFICATION AND STATISTICAL ANALYSIS

SUPPLEMENTAL INFORMATION

Supplemental information can be found online at https://doi.org/10.1016/j.celrep.2025.115353.

Received: August 1, 2024
Revised: December 17, 2024
Accepted: February 5, 2025
Published: February 26, 2025

REFERENCES

1. Cappadocia, L., and Lima, C.D. (2018). Ubiquitin-like Protein Conjugation: Structures, Chemistry, and Mechanism. Chem. Rev. *118*, 889–918.
2. Vertegaal, A.C.O. (2022). Signalling mechanisms and cellular functions of SUMO. Nat. Rev. Mol. Cell Biol. *23*, 715–731.
3. Jentsch, S., and Psakhye, I. (2013). Control of nuclear activities by substrate-selective and protein-group SUMOylation. Annu. Rev. Genet. *47*, 167–186.
4. Lascorz, J., Codina-Fabra, J., Reverter, D., and Torres-Rosell, J. (2022). SUMO-SIM interactions: From structure to biological functions. Semin. Cell Dev. Biol. *132*, 193–202.
5. Yau, T.Y., Sander, W., Eidson, C., and Courey, A.J. (2021). SUMO Interacting Motifs: Structure and Function. Cell *10*, 2825.
6. González-Prieto, R., Eifler-Olivi, K., Claessens, L.A., Willemstein, E., Xiao, Z., Talavera Ormeno, C.M.P., Ovaa, H., Ulrich, H.D., and Vertegaal, A.C.O. (2021). Global non-covalent SUMO interaction networks reveal SUMO-dependent stabilization of the non-homologous end joining complex. Cell Rep. *34*, 108691.
7. Aguilar-Martinez, E., Chen, X., Webber, A., Mould, A.P., Seifert, A., Hay, R.T., and Sharrocks, A.D. (2015). Screen for multi-SUMO-binding proteins reveals a multi-SIM-binding mechanism for recruitment of the transcriptional regulator ZMYM2 to chromatin. Proc. Natl. Acad. Sci. USA *112*, E4854–E4863.
8. Meulmeester, E., Kunze, M., Hsiao, H.H., Urlaub, H., and Melchior, F. (2008). Mechanism and consequences for paralog-specific sumoylation of ubiquitin-specific protease 25. Mol. Cell *30*, 610–619.
9. Chang, C.C., Naik, M.T., Huang, Y.S., Jeng, J.C., Liao, P.H., Kuo, H.Y., Ho, C.C., Hsieh, Y.L., Lin, C.H., Huang, N.J., et al. (2011). Structural and functional roles of Daxx SIM phosphorylation in SUMO paralog-selective binding and apoptosis modulation. Mol. Cell *42*, 62–74.
10. Hua, D., and Wu, X. (2022). Small-molecule inhibitors targeting small ubiquitin-like modifier pathway for the treatment of cancers and other diseases. Eur. J. Med. Chem. *233*, 114227.
11. Hirohama, M., Kumar, A., Fukuda, I., Matsuoka, S., Igarashi, Y., Saitoh, H., Takagi, M., Shin-ya, K., Honda, K., Kondoh, Y., et al. (2013). Spectomycin B1 as a novel SUMOylation inhibitor that directly binds to SUMO E2. ACS Chem. Biol. *8*, 2635–2642.
12. Becker, J., Barysch, S.V., Karaca, S., Dittner, C., Hsiao, H.H., Berriel Diaz, M., Herzig, S., Urlaub, H., and Melchior, F. (2013). Detecting endogenous SUMO targets in mammalian cells and tissues. Nat. Struct. Mol. Biol. *20*, 525–531.
13. Hendriks, I.A., Lyon, D., Su, D., Skotte, N.H., Daniel, J.A., Jensen, L.J., and Nielsen, M.L. (2018). Site-specific characterization of endogenous SUMOylation across species and organs. Nat. Commun. *9*, 2456.
14. Seufert, W., Futcher, B., and Jentsch, S. (1995). Role of a ubiquitin-conjugating enzyme in degradation of S- and M-phase cyclins. Nature *373*, 78–81.
15. Helma, J., Cardoso, M.C., Muyldermans, S., and Leonhardt, H. (2015). Nanobodies and recombinant binders in cell biology. J. Cell Biol. *209*, 633–644.
16. Gilbreth, R.N., Truong, K., Madu, I., Koide, A., Wojcik, J.B., Li, N.S., Piccirilli, J.A., Chen, Y., and Koide, S. (2011). Isoform-specific monobody inhibitors of small ubiquitin-related modifiers engineered using structure-guided library design. Proc. Natl. Acad. Sci. USA *108*, 7751–7756.
17. Hughes, D.J., Tiede, C., Penswick, N., Tang, A.A.S., Trinh, C.H., Mandal, U., Zajac, K.Z., Gaule, T., Howell, G., Edwards, T.A., et al. (2017). Generation of specific inhibitors of SUMO-1- and SUMO-2/3-mediated protein-protein interactions using Affimer (Adhiron) technology. Sci. Signal. *10*, eaaj2005.
18. Plückthun, A. (2015). Designed ankyrin repeat proteins (DARPins): binding proteins for research, diagnostics, and therapy. Annu. Rev. Pharmacol. Toxicol. *55*, 489–511.
19. Cappadocia, L., Kochańczyk, T., and Lima, C.D. (2021). DNA asymmetry promotes SUMO modification of the single-stranded DNA-binding protein RPA. EMBO. J. *40*, e103787.
20. Cremona, C.A., Sarangi, P., Yang, Y., Hang, L.E., Rahman, S., and Zhao, X. (2012). Extensive DNA damage-induced sumoylation contributes to replication and repair and acts in addition to the mec1 checkpoint. Mol. Cell *45*, 422–432.
21. Psakhye, I., and Jentsch, S. (2012). Protein group modification and synergy in the SUMO pathway as exemplified in DNA repair. Cellule *151*, 807–820.
22. Dreier, B., and Plückthun, A. (2012). Rapid selection of high-affinity binders using ribosome display. Methods Mol. Biol. *805*, 261–286.
23. Binz, H.K., Stumpp, M.T., Forrer, P., Amstutz, P., and Plückthun, A. (2003). Designing repeat proteins: well-expressed, soluble and stable proteins from combinatorial libraries of consensus ankyrin repeat proteins. J. Mol. Biol. *332*, 489–503.
24. Binz, H.K., Amstutz, P., and Plückthun, A. (2005). Engineering novel binding proteins from nonimmunoglobulin domains. Nat. Biotechnol. *23*, 1257–1268.
25. Plückthun, A. (2012). Ribosome display: a perspective. Methods Mol. Biol. *805*, 3–28.
26. Binz, H.K., Kohl, A., Plückthun, A., and Grütter, M.G. (2006). Crystal structure of a consensus-designed ankyrin repeat protein: implications for stability. Proteins *65*, 280–284.
27. Hoege, C., Pfander, B., Moldovan, G.L., Pyrowolakis, G., and Jentsch, S. (2002). RAD6-dependent DNA repair is linked to modification of PCNA by ubiquitin and SUMO. Nature *419*, 135–141.
28. Windecker, H., and Ulrich, H.D. (2008). Architecture and assembly of poly-SUMO chains on PCNA in Saccharomyces cerevisiae. J. Mol. Biol. *376*, 221–231.
29. Parker, J.L., Bucceri, A., Davies, A.A., Heidrich, K., Windecker, H., and Ulrich, H.D. (2008). SUMO modification of PCNA is controlled by DNA. EMBO J. *27*, 2422–2431.
30. Knipscheer, P., Flotho, A., Klug, H., Olsen, J.V., van Dijk, W.J., Fish, A., Johnson, E.S., Mann, M., Sixma, T.K., and Pichler, A. (2008). Ubc9 sumoylation regulates SUMO target discrimination. Mol. Cell *31*, 371–382.
31. Johnson, E.S., and Gupta, A.A. (2001). An E3-like factor that promotes SUMO conjugation to the yeast septins. Cell *106*, 735–744.
32. Tatham, M.H., and Hay, R.T. (2009). FRET-based in vitro assays for the analysis of SUMO protease activities. Methods Mol. Biol. *497*, 253–268.
33. Stankovic-Valentin, N., Kozaczkiewicz, L., Curth, K., and Melchior, F. (2009). An in vitro FRET-based assay for the analysis of SUMO conjugation and isopeptidase cleavage. Methods Mol. Biol. *497*, 241–251.
34. Mossessova, E., and Lima, C.D. (2000). Ulp1-SUMO crystal structure and genetic analysis reveal conserved interactions and a regulatory element essential for cell growth in yeast. Mol. Cell *5*, 865–876.
35. Li, S.J., and Hochstrasser, M. (1999). A new protease required for cell-cycle progression in yeast. Nature *398*, 246–251.
36. Sun, H., Leverson, J.D., and Hunter, T. (2007). Conserved function of RNF4 family proteins in eukaryotes: targeting a ubiquitin ligase to SUMOylated proteins. EMBO J. *26*, 4102–4112.
37. Prudden, J., Pebernard, S., Raffa, G., Slavin, D.A., Perry, J.J.P., Tainer, J.A., McGowan, C.H., and Boddy, M.N. (2007). SUMO-targeted ubiquitin ligases in genome stability. EMBO J. *26*, 4089–4101.
38. Sheng, W., and Liao, X. (2002). Solution structure of a yeast ubiquitin-like protein Smt3: the role of structurally less defined sequences in protein-protein recognitions. Protein Sci. *11*, 1482–1491.

39. Armstrong, A.A., Mohideen, F., and Lima, C.D. (2012). Recognition of SUMO-modified PCNA requires tandem receptor motifs in Srs2. Nature *483*, 59–63.

40. Lois, L.M., and Lima, C.D. (2005). Structures of the SUMO E1 provide mechanistic insights into SUMO activation and E2 recruitment to E1. EMBO J. *24*, 439–451.

41. Duda, D.M., van Waardenburg, R.C.A.M., Borg, L.A., McGarity, S., Nourse, A., Waddell, M.B., Bjornsti, M.A., and Schulman, B.A. (2007). Structure of a SUMO-binding-motif mimic bound to Smt3p-Ubc9p: conservation of a non-covalent ubiquitin-like protein-E2 complex as a platform for selective interactions within a SUMO pathway. J. Mol. Biol. *369*, 619–630.

42. Streich, F.C., Jr., and Lima, C.D. (2016). Capturing a substrate in an activated RING E3/E2-SUMO complex. Nature *536*, 304–308.

43. Bellí, G., Garí, E., Piedrafita, L., Aldea, M., and Herrero, E. (1998). An activator/repressor dual system allows tight tetracycline-regulated gene expression in budding yeast. Nucleic. Acids. Res. *26*, 942–947.

44. Johnson, E.S., and Blobel, G. (1999). Cell cycle-regulated attachment of the ubiquitin-related protein SUMO to the yeast septins. J. Cell Biol. *147*, 981–994.

45. Dhingra, N., Wei, L., and Zhao, X. (2019). Replication protein A (RPA) sumoylation positively influences the DNA damage checkpoint response in yeast. J. Biol. Chem. *294*, 2690–2699.

46. Mao, Y., Sun, M., Desai, S.D., and Liu, L.F. (2000). SUMO-1 conjugation to topoisomerase I: A possible repair response to topoisomerase-mediated DNA damage. Proc. Natl. Acad. Sci. USA *97*, 4046–4051.

47. Bachant, J., Alcasabas, A., Blat, Y., Kleckner, N., and Elledge, S.J. (2002). The SUMO-1 isopeptidase Smt4 is linked to centromeric cohesion through SUMO-1 modification of DNA topoisomerase II. Mol. Cell *9*, 1169–1182.

48. Silver, H.R., Nissley, J.A., Reed, S.H., Hou, Y.M., and Johnson, E.S. (2011). A role for SUMO in nucleotide excision repair. DNA Repair *10*, 1243–1251.

49. Freudenreich, C.H., and Su, X.A. (2016). Relocalization of DNA lesions to the nuclear pore complex. FEMS Yeast Res. *16*, fow095.

50. Horigome, C., Bustard, D.E., Marcomini, I., Delgoshaie, N., Tsai-Pflugfelder, M., Cobb, J.A., and Gasser, S.M. (2016). PolySUMOylation by Siz2 and Mms21 triggers relocation of DNA breaks to nuclear pores through the Slx5/Slx8 STUbL. Genes Dev. *30*, 931–945.

51. Whalen, J.M., Dhingra, N., Wei, L., Zhao, X., and Freudenreich, C.H. (2020). Relocation of Collapsed Forks to the Nuclear Pore Complex Depends on Sumoylation of DNA Repair Proteins and Permits Rad51 Association. Cell Rep. *31*, 107635.

52. Yong-Gonzales, V., Hang, L.E., Castellucci, F., Branzei, D., and Zhao, X. (2012). The Smc5-Smc6 complex regulates recombination at centromeric regions and affects kinetochore protein sumoylation during normal growth. PLoS One *7*, e51540.

53. Sogo, J.M., Lopes, M., and Foiani, M. (2002). Fork reversal and ssDNA accumulation at stalled replication forks owing to checkpoint defects. Science *297*, 599–602.

54. Wong, R.P., García-Rodríguez, N., Zilio, N., Hanulová, M., and Ulrich, H.D. (2020). Processing of DNA Polymerase-Blocking Lesions during Genome Replication Is Spatially and Temporally Segregated from Replication Forks. Mol. Cell *77*, 3–16.e4.

55. Giannattasio, M., Follonier, C., Tourrière, H., Puddu, F., Lazzaro, F., Pasero, P., Lopes, M., Plevani, P., and Muzi-Falconi, M. (2010). Exo1 competes with repair synthesis, converts NER intermediates to long ssDNA gaps, and promotes checkpoint activation. Mol. Cell *40*, 50–62.

56. Kumar, A., Mathew, V., and Stirling, P.C. (2022). Nuclear protein quality control in yeast: The latest INQuiries. J. Biol. Chem. *298*, 102199.

57. Dieckhoff, P., Bolte, M., Sancak, Y., Braus, G.H., and Irniger, S. (2004). Smt3/SUMO and Ubc9 are required for efficient APC/C-mediated proteolysis in budding yeast. Mol. Microbiol. *51*, 1375–1387.

58. Raman, N., Nayak, A., and Muller, S. (2013). The SUMO system: a master organizer of nuclear protein assemblies. Chromosoma *122*, 475–485.

59. Hendriks, I.A., Treffers, L.W., Verlaan-de Vries, M., Olsen, J.V., and Vertegaal, A.C.O. (2015). SUMO-2 Orchestrates Chromatin Modifiers in Response to DNA Damage. Cell Rep. *10*, 1778–1791.

60. Branzei, D., Sollier, J., Liberi, G., Zhao, X., Maeda, D., Seki, M., Enomoto, T., Ohta, K., and Foiani, M. (2006). Ubc9- and mms21-mediated sumoylation counteracts recombinogenic events at damaged replication forks. Cell *127*, 509–522.

61. Liang, J., Li, B.Z., Tan, A.P., Kolodner, R.D., Putnam, C.D., and Zhou, H. (2018). SUMO E3 ligase Mms21 prevents spontaneous DNA damage induced genome rearrangements. PLoS Genet. *14*, e1007250.

62. Bonner, J.N., Choi, K., Xue, X., Torres, N.P., Szakal, B., Wei, L., Wan, B., Arter, M., Matos, J., Sung, P., et al. (2016). Smc5/6 Mediated Sumoylation of the Sgs1-Top3-Rmi1 Complex Promotes Removal of Recombination Intermediates. Cell Rep. *16*, 368–378.

63. Stelter, P., and Ulrich, H.D. (2003). Control of spontaneous and damage-induced mutagenesis by SUMO and ubiquitin conjugation. Nature *425*, 188–191.

64. Papouli, E., Chen, S., Davies, A.A., Huttner, D., Krejci, L., Sung, P., and Ulrich, H.D. (2005). Crosstalk between SUMO and ubiquitin on PCNA is mediated by recruitment of the helicase Srs2p. Mol. Cell *19*, 123–133.

65. Pleiner, T., Bates, M., Trakhanov, S., Lee, C.T., Schliep, J.E., Chug, H., Böhning, M., Stark, H., Urlaub, H., and Görlich, D. (2015). Nanobodies: site-specific labeling for super-resolution imaging, rapid epitope-mapping and native protein complex isolation. Elife *4*, e11349.

66. Finley, D., Ozkaynak, E., and Varshavsky, A. (1987). The yeast polyubiquitin gene is essential for resistance to high temperatures, starvation, and other stresses. Cell *48*, 1035–1046.

67. Kabsch, W. (2010). Xds. Acta. Crystallogr. D. Biol. Crystallogr. *66*, 125–132.

68. Evans, P. (2006). Scaling and assessment of data quality. Acta Crystallogr. D Biol. Crystallogr. *62*, 72–82.

69. Agirre, J., Atanasova, M., Bagdonas, H., Ballard, C.B., Baslé, A., Beilsten-Edmands, J., Borges, R.J., Brown, D.G., Burgos-Mármol, J.J., Berrisford, J.M., et al. (2023). The CCP4 suite: integrative software for macromolecular crystallography. Acta Crystallogr. D Struct. Biol. *79*, 449–461.

70. Evans, P.R., and Murshudov, G.N. (2013). How good are my data and what is the resolution? Acta Crystallogr. D Biol. Crystallogr. *69*, 1204–1214.

71. McCoy, A.J., Grosse-Kunstleve, R.W., Adams, P.D., Winn, M.D., Storoni, L.C., and Read, R.J. (2007). Phaser crystallographic software. J. Appl. Crystallogr. *40*, 658–674.

72. Liebschner, D., Afonine, P.V., Baker, M.L., Bunkóczi, G., Chen, V.B., Croll, T.I., Hintze, B., Hung, L.W., Jain, S., McCoy, A.J., et al. (2019). Macromolecular structure determination using X-rays, neutrons and electrons: recent developments in Phenix. Acta Crystallogr. D Struct. Biol. *75*, 861–877.

73. Cowtan, K. (2006). The Buccaneer software for automated model building. 1. Tracing protein chains. Acta Crystallogr. D Biol. Crystallogr. *62*, 1002–1011.

74. Emsley, P., and Cowtan, K. (2004). Coot: model-building tools for molecular graphics. Acta Crystallogr. D Biol. Crystallogr. *60*, 2126–2132.

75. Murshudov, G.N., Vagin, A.A., and Dodson, E.J. (1997). Refinement of macromolecular structures by the maximum-likelihood method. Acta Crystallogr. D Biol. Crystallogr. *53*, 240–255.

76. Afonine, P.V., Grosse-Kunstleve, R.W., Echols, N., Headd, J.J., Moriarty, N.W., Mustyakimov, M., Terwilliger, T.C., Urzhumtsev, A., Zwart, P.H., and Adams, P.D. (2012). Towards automated crystallographic structure refinement with phenix.refine. Acta Crystallogr. D Biol. Crystallogr. *68*, 352–367.

77. Krissinel, E., and Henrick, K. (2007). Inference of macromolecular assemblies from crystalline state. J. Mol. Biol. *372*, 774–797.

78. Edgar, R.C. (2004). MUSCLE: multiple sequence alignment with high accuracy and high throughput. Nucleic Acids Res. *32*, 1792–1797.

79. Brauchle, M., Hansen, S., Caussinus, E., Lenard, A., Ochoa-Espinosa, A., Scholz, O., Sprecher, S.G., Plückthun, A., and Affolter, M. (2014). Protein interference applications in cellular and developmental biology using DARPins that recognize GFP and mCherry. Biol. Open *3*, 1252–1261.

80. Kramer, M.A., Wetzel, S.K., Plückthun, A., Mittl, P.R.E., and Grütter, M.G. (2010). Structural determinants for improved stability of designed ankyrin repeat proteins with a redesigned C-capping module. J. Mol. Biol. *404*, 381–391.

81. Schilling, J., Schöppe, J., and Plückthun, A. (2014). From DARPins to LoopDARPins: novel LoopDARPin design allows the selection of low picomolar binders in a single round of ribosome display. J. Mol. Biol. *426*, 691–721.

82. Zahnd, C., Sarkar, C.A., and Plückthun, A. (2010). Computational analysis of off-rate selection experiments to optimize affinity maturation by directed evolution. Protein Eng. Des. Sel. *23*, 175–184.

83. Strubel, A., Münick, P., Chaikuad, A., Dreier, B., Schaefer, J., Gebel, J., Osterburg, C., Tuppi, M., Schäfer, B., Knapp, S., et al. (2022). Designed Ankyrin Repeat Proteins as a tool box for analyzing p63. Cell Death Differ. *29*, 2445–2458.

84. Parker, J.L., and Ulrich, H.D. (2012). In vitro PCNA modification assays. Methods Mol. Biol. *920*, 569–589.

85. Parker, J.L., and Ulrich, H.D. (2012). A SUMO-interacting motif activates budding yeast ubiquitin ligase Rad18 towards SUMO-modified PCNA. Nucleic Acids Res. *40*, 11380–11388.

86. Wegmann, S., Meister, C., Renz, C., Yakoub, G., Wollscheid, H.P., Takahashi, D.T., Mikicic, I., Beli, P., and Ulrich, H.D. (2022). Linkage reprogramming by tailor-made E3s reveals polyubiquitin chain requirements in DNA-damage bypass. Mol. Cell *82*, 1589–1602.e5.

87. Petris, G., Vecchi, L., Bestagno, M., and Burrone, O.R. (2011). Efficient detection of proteins retro-translocated from the ER to the cytosol by in vivo biotinylation. PLoS One *6*, e23712.

88. Werner, A., Moutty, M.C., Möller, U., and Melchior, F. (2009). Performing in vitro sumoylation reactions using recombinant enzymes. Methods Mol. Biol. *497*, 187–199.

89. Plechanovová, A., Jaffray, E.G., McMahon, S.A., Johnson, K.A., Navratilova, I., Naismith, J.H., and Hay, R.T. (2011). Mechanism of ubiquitylation by dimeric RING ligase RNF4. Nat. Struct. Mol. Biol. *18*, 1052–1059.

90. Morawska, M., and Ulrich, H.D. (2013). An expanded tool kit for the auxin-inducible degron system in budding yeast. Yeast *30*, 341–351.

STAR★METHODS

KEY RESOURCES TABLE

REAGENT or RESOURCE	SOURCE	IDENTIFIER
Antibodies		
Anti-mCherry, mouse mAb/IgG2a (clone 1C51)	Abcam	Cat# ab125096; RRID: AB_11133266
Anti-GFP, mouse mAb/IgG1κ (clone 7.1/13.1)	Roche	Cat# 118114460001; RRID: AB_390913
Anti-PCNA (*S. cerevisiae*), rabbit polyclonal	Stelter & Ulrich[63]	N/A
Anti-RNF4, goat polyclonal IgG, affinity-purified	Bio-Techne	Cat# AF7964
Anti-Smt3 (*S. cerevisiae*), rabbit polyclonal	Papouli et al.[64]	N/A
Anti-tubulin α-chain, rabbit mAb/IgG (clone EPR13799)	Abcam	Cat# ab184970; RRID: AB_2928998
Anti-GFP nanobody, Atto 488	Pleiner et al.[65]	N/A
Anti-goat IgG, donkey, IRDye 800CW	LI-COR	Cat# 926-32214
Anti-mouse IgG, donkey, IRDye 680LT	LI-COR	Cat# 926-68022
Anti-mouse IgG, donkey, IRDye 800CW	LI-COR	Cat# 926-32212
Anti-mouse IgG, goat, HRP	Pierce	Cat# 1858413
Anti-rabbit IgG, donkey, IRDye 680LT	LI-COR	Cat# 926-68023
Anti-rabbit IgG, goat, IRDye 800CW	LI-COR	Cat# 926-32211
Anti-rabbit IgG, goat, HRP	Agilent Technologies	Cat# P0448; RRID: AB_2617138
Anti-rabbit IgG (H+L), goat, Alexa Fluor 594	Thermo Fisher Scientific	Cat# A11012
Bacterial strains		
Escherichia coli TOP10	Thermo Fisher Scientific	Cat# C404010
Escherichia coli XL1-Blue	Agilent Technologies	Cat# 200249
Escherichia coli BL21 (DE3)	Merck KGaA	Cat# 69450-3
Escherichia coli Rosetta™ 2(DE3) pLysS	Merck KGaA	Cat# 71403-3
Escherichia coli BL21 CodonPlus (DE3)-RIL	Agilent Technologies	Cat# 230245
Chemicals, peptides, and recombinant proteins		
Bovine serum albumin (BSA)	Merck KGaA	Cat# A7906
Ni-NTA agarose	Qiagen	Cat# 30250
Streptavidin agarose	Thermo Fisher Scientific	Cat# 20353
Sulfolink resin	Thermo Fisher Scientific	Cat# 20401
SIGMAFAST Protease Inhibitor Cocktail	Merck KGaA	Cat# S8830
Imidazole	Merck KGaA	Cat# I2399
Isopropyl b-D-1-thiogalactopyranoside (IPTG)	Generon	Cat# GEN-S-02122
Dithiothreitol (DTT)	Merck KGaA	Cat# D0632
N-ethylmaleimide (NEM)	Merck KGaA	Cat# E3876
IGEPAL CA-630	Sigma-Aldrich	Cat# I8896
Triton X-100	Merck KGaA	Cat# T9284
MagStrep Strep-Tactin XT beads	IBA-Lifesciences GmbH	Cat# 2-5090-002
TEV protease	In-house	N/A
Zymolyase T100	Carl Roth	Cat# 9329.2
4',6-diamidin-2-phenylindol (DAPI)	Sigma-Aldrich	Cat# 10236276001
ProLong Diamond mounting medium	Thermo Fisher Sicentific	Cat# P36961
Concanavalin A	Sigma-Aldrich	Cat# L7647

(*Continued on next page*)

Continued		
REAGENT or RESOURCE	SOURCE	IDENTIFIER
Lipsol	DynalonLabware	Cat# 504004-0000
Photo-Flo 200	Thermo Fisher Scientific	Cat# 50-268-05
Critical commercial assays		
Superdex 75 10/300 GL column	Cytiva	Cat# 17-5174-01
HiTrap Q HP, 5 mL	Cytiva	Cat# 17-1154-01
HiTrap SP FF, 5 mL	Cytiva	Cat# 17-5054-01
Mono Q 10/100 GL	Cytiva	Cat# 17-5166-01
PD-10 desalting columns	Cytiva	Cat# 17-0851-01
HBS-EP buffer	Cytiva	Cat# BR100669
Biotin capture kit	Cytiva	Cat# 28920233
Deposited data		
Atomic coordinates of A10·Smt3 complex	This study	PDB: 9G8I
Atomic coordinates of A10·Smt3 complex	This study	PDB: 9GAU
Experimental models: Organisms/strains		
Saccharomyces cerevisiae: strain background DF5	Finley et al.[66]	N/A
Other yeast strains: see supplemental information	This study	Table S2
Oligonucleotides		
See supplemental information	This study	Table S3
Recombinant DNA		
See supplemental information	This study	Table S4
Software and algorithms		
Biacore Evaluation Software 2.0.2	Cytiva	N/A
Image Studio 3.1	LI-COR	N/A
Prism 8	GraphPad	N/A
BD FACSDIVA software	BD Biosciencies	N/A
FlowJo™ v10.10	BD Life Sciences	N/A
SoftWoRx	GE Healthcare	N/A
XDS	Kabsch[67]	N/A
POINTLESS	Evans[68]; Agirre et al.[69]	N/A
AIMLESS	Agirre et al.[69]; Evans & Murshudov[70]	N/A
Phaser	McCoy et al.[71]	N/A
PHENIX	Liebschner et al.[72]	N/A
CCP4	Agirre et al.[69]	N/A
Buccaneer	Cowtan[73]	N/A
Coot	Emsley & Cowtan[74]	N/A
Refmac	Agirre et al.[69]; Murshudov et al.[75]	N/A
PHENIX	Liebschner et al.[72]; Afonine et al.[76]	N/A
PDBe PISA v1.52	Krissinel & Henrick[77]	N/A
PyMOL version 2.5.8	Molecular Graphics System, Schrödinger, LLC	N/A
MUSCLE 3.8	Edgar[78]	N/A

EXPERIMENTAL MODEL AND STUDY PARTICIPANTS DETAILS

S. cerevisiae strains used in this study are listed in Table S2. All strains were grown at 30°C with agitation at 200 rpm, except for the temperature-sensitive *ubc9*^{ts} mutant, which was grown at 25°C (permissive temperature) or 37°C (restrictive temperature). Strains harboring integrated expression constructs were grown in SC-complete or YPD medium using 2% (w/v) glucose as a carbon source.

Strain construction was accomplished by transformation of plasmids, tagging or deletion cassettes or by mating and tetrad dissection.

METHOD DETAILS

Construction of plasmids

Genes of interest were inserted into expression vectors using restriction cloning or Gibson assembly. All constructs were propagated in *Escherichia coli* TOP10 and verified by Sanger sequencing.

DARPin selection and initial screening

The target Smt3 (UniProt: Q12306), fused to an N-terminal MAH_6 and Twin-Strep tag in the vector pQIq (a derivative of pQE30, Qiagen), was expressed in *E. coli* XL1-Blue and purified by Ni-NTA chromatography. To generate DARPin binders for Smt3, Smt3 was immobilized on MagStrep Strep-Tactin XT beads and not by biotinylation as normally performed. Ribosome display selection was otherwise performed as previously described,[22] but using a semiautomatic KingFisher Flex MTP 96 well platform.

The fully synthetic library included N3C-DARPins with three randomized internal repeats with the original randomization strategy as reported,[23] but including a stabilized C-cap.[18,79,80] Additionally, the library is a 1:1 mixture of DARPins with randomized and non-randomized N- and C-caps, respectively,[18,81] and successively enriched pools were ligated in a ribosome display-specific vector.[22]

Selection was performed over four rounds with decreasing concentrations of Smt3 (250 pmol, 125 pmol, 5 pmol, and finally 50 pmol of target as a recovery round) and increasing washing steps for the first three cycles.[22,82] For rounds 2 to 4, pre-panning with MagStrep Strep-Tactin XT beads was performed for the Smt3 selection to avoid Strep-Tactin binders.

To screen individual DARPins for their binding properties, the selected pool of DARPins from ribosome display was subcloned by restriction digest with *Bam*HI and *Hin*dIII into the vector pQIq. This creates DARPins with an N- terminal $MRGS(H)_6$-tag and a C-terminal FLAG-tag. 380 single clones were screened for binding to a biotinylated version of Smt3 using homogeneous time-resolved fluorescence HTRF, performed according to a previously established protocol.[83] After sequencing 33 single clones, a total of 19 unique DARPins were obtained binding to Smt3.

Preparation of recombinant proteins

Unless otherwise noted, His-tagged proteins were purified by a standard protocol involving Ni-NTA affinity chromatography in a batch procedure using HEPES- or Tris-based buffer, followed by gel filtration on a Superdex 75 10/300 GL column in a buffer suitable for the relevant downstream application. Purified proteins were stored at -70°C. $Ubc9^{His}$ and $Ubc9(K153R)^{His}$ were purified as described.[84] ^{His}Siz1(1-508) was purified as previously described.[85] ^{His}Ulp1(403-621) was purified as previously described.[86] ^{His}PCNA and His-tagged RFC complex were purified essentially as described.[29]

DARPins

$^{His}DARPin^{FLAG}$ proteins were produced in *Escherichia coli* BL21 DE3 via addition of 0.75 mM IPTG for 4 h at 37°C. Cells were lysed by sonication on ice in HEPES lysis buffer (40 mM HEPES pH 7.5, 150 mM NaCl, 20 mM imidazole, 1 mM DTT, SIGMAFAST Protease Inhibitor Cocktail). After purification according to the standard protocol, DARPins were stored in the relevant buffer for downstream applications.

$^{His\text{-}AVI}$Smt3, biotinylated Smt3, hSUMO1, and hSUMO2

Biotinylated Smt3 was produced in *E. coli* Rosetta pLysS by co-transformation of the $^{His\text{-}AVI}$Smt3 expression plasmid with an expression plasmid encoding BirA. Briefly, a small overnight culture was grown in LB medium with the appropriate antibiotics at 37°C. This culture was diluted to an OD_{600} of 0.1 in LB media with antibiotics and grown to an OD_{600} of 0.7-0.8. Biotin was then added to 50 μM from a solution prepared by mixing 12 mg of D-biotin with 10 mL of warm 10 mM Bicine buffer (pH 8.3) and filter-sterilization. At the same time, expression was induced by addition of 50 μM IPTG for 6 h at 30°C. After lysis by sonication, SIGMAFAST Protease Inhibitor Cocktail was added, and biotinylated $^{His\text{-}AVI}$Smt3 was purified via Ni-NTA affinity chromatography and gel filtration in HBS-EP buffer.

The degree of biotinylation was analyzed by a gel-based streptavidin shift assay.[87] Biotinylated protein (0.2 to 5 μg) was incubated in 1x SDS loading buffer for 10 min at 95°C. Samples were cooled to room temperature and 1 μL of streptavidin solution (1 mg/mL in PBS) was added. Samples were incubated for 30 min at room temperature and analyzed by SDS-PAGE. Biotinylation was quantified by comparing the streptavidin-containing samples with control samples without streptavidin, using Image-J software.

Where immobilization via Streptavidin was not needed, $^{His\text{-}AVI}$Smt3 was purified in the same manner, but without BirA-mediated *in vivo* biotinylation.

Untagged Smt3(20-98) and Smt3(K11/15/19R)

For crystallization purposes, Smt3(20-98) was produced in *E. coli* BL21 Codon Plus via addition of 0.2 mM IPTG for 4 h at 37°C. Cells were lysed by sonification in Tris lysis buffer (25 mM Tris-HCl pH 7.5, 50 mM NaCl, 0.5 mM EDTA, 1 mM DTT, SIGMAFAST Protease Inhibitor Cocktail). The cleared lysate was passed through a 0.45 μM filter and loaded onto an anion exchange column (HiTrap Q, 5 mL) equilibrated in buffer A (25 mM Tris-HCl pH 7.5, 0.5 mM DTT, 1 mM EDTA) + 40 mM NaCl. Bound proteins were eluted with a gradient of NaCl (100-700 mM). Relevant fractions were pooled and buffer-exchanged to buffer A + 40 mM NaCl. After passage through a cation exchange column (HiTrap SP, 5 mL) equilibrated in buffer A + 40 mM NaCl, the protein was subjected to gel filtration

in crystallization buffer (40 mM HEPES pH 7.4, 50 mM NaCl, 1 mM DTT). Untagged Smt3(K11/15/19R) was purified in the same manner.

$^{His\text{-}YFP}$Smt3 and $^{His\text{-}CFP}$GAPtail

FRET partner proteins were produced essentially as described,[33] with the following modifications: expression was induced in *E. coli* BL21 Codon Plus via addition of 0.4 mM IPTG for 5 h at 20°C. After lysis by sonication in a buffer containing 50 mM Tris-HCl, 50 mM NaCl, 1 mM EDTA, pH 8.0, 1 mM DTT, SIGMAFAST Protease Inhibitor Cocktail, proteins were first subjected to Ni-NTA affinity purification, followed by gel filtration in 20 mM HEPES, 110 mM potassium acetate, 2 mM magnesium acetate, 1 mM EGTA, pH 7.3, 1 mM DTT, SIGMAFAST Protease Inhibitor Cocktail. Peak fractions were concentrated to 1 mg/mL and flash-frozen.

E1

The ^{His}Aos1·Uba2 complex was produced essentially as described,[88] with the following modifications: induction was for 5 h at 25°C with 0.1 mM IPTG. Lysis was performed by two passages over a high-pressure cell disruption system (1.8 mPa, 4°C). The cleared supernatant was applied to 2 mL Ni-NTA agarose. Bound proteins were eluted with five aliquots of 2 mL elution buffer. After a gel filtration step, relevant fractions were loaded onto an anion exchange column (Mono Q 10/100 GL) equilibrated in 50 mM Tris-HCl pH 7.5, 50 mM NaCl, 1 mM DTT, and eluted using a linear gradient (20 column volumes) of 50 to 500 mM NaCl. E1-containing fractions were buffer-exchanged via a PD10 column into storage buffer (20 mM HEPES pH 7.3, 110 mM potassium acetate, 2 mM magnesium acetate, 1 mM EGTA, 1 mM DTT, SIGMAFAST Protease Inhibitor Cocktail), and flash-frozen in aliquots.

RNF4

$^{His\text{-}MBP}$RNF4 was produced as described,[89] except that a batch method was used for the Ni-NTA purification (500 μL Ni-NTA beads per 500 mL culture, 2 h incubation at 4°C, followed by three washes and five elution steps). The MBP tag was removed by cleavage with TEV protease at 4°C overnight. After a step of reverse Ni-NTA purification to remove His-MBP and His-TEV, the cleaved RNF4 protein was subjected to a final step of gel filtration.

Sequence analysis

DARPin sequences were subjected to multiple alignment using MUSCLE 3.8.[78]

In vitro interaction assays

Pull-down assays with recombinant proteins

Purified $^{His\text{-}Cys}$Smt3 and its variants were coupled to Sulfolink resin according to the manufacturer's protocol, using 0.6 nmol protein per 5 μL of slurry. Pull-down assays were performed with purified DARPins, using 0.3 nmol bait on beads and 0.1 nmol DARPin per reaction in phosphate-buffered saline (PBS) containing 0.1% Triton X-100. After a 1 h incubation at 4°C followed by washes with the same buffer, bound material was analyzed by SDS-PAGE and Coomassie staining.

Pull-down assay with yeast lysate

Total lysate was prepared by means of a high-pressure cell disruption system (35,000 psi, 3 rounds at 4°C) in a buffer containing 50 mM Tris pH 7.5, 150 mM NaCl, 10 % (v/v) glycerol, 1 mM DTT, 5 mM EDTA, 10 mM N-ethylmaleimide, and SIGMAFAST Protease Inhibitor Cocktail. Following centrifugation at 300 x *g* for 5 min at 4°C, 0.5 % (v/v) IGEPAL and 0.25 % (v/v) Triton X-100 were added to the cleared lysate. The extract was incubated for 1 h at 4°C with agitation on a roller, centrifuged at 20,000 x *g* for 30 min at 4°C, and the protein concentration of the supernatant was determined. The lysate was stored at -70°C. Ni-NTA agarose beads (15 μL per sample) were pre-incubated with DARPins for 60-90 min at 4°C on a rotation wheel. After washing with 50 mM HEPES pH 7.4, 50 mM NaCl, 1% (v/v) glycerol, 1% (v/v) Triton X-100, blocking for 30 min at 4°C with 1 mg/mL BSA and renewed washing, beads were incubated with 10 mg yeast lysate for 90 min at 4°C. Samples were washed again with the same buffer, and bound protein was eluted by addition of 15 μL 1xLDS and heating at 95°C for 5 min. Eluted protein, input and unbound material were analyzed by SDS-PAGE and western blotting using a polyclonal anti-Smt3 antibody.

Analytical gel filtration

Analytical gel filtration was performed on a Superdex 75 10/300 column in 40 mM Na-HEPES pH 7.4, 50 mM NaCl, 8 mM magnesium acetate. DARPins and Smt3 were applied at 5 μM each after incubation separately or together at 4°C overnight.

Determination of binding parameters

Interactions of DARPins with Smt3 were quantified by surface plasmon resonance measurements using a Biacore X-100 instrument (Cytiva). Steady-state affinity measurements were performed by immobilizing 200-500 RU of biotinylated $^{His\text{-}AVI}$Smt3 or mutants on a Streptavidin-coated chip using a Biotin capture kit. For kinetic analysis of association and dissociation constants, 50-100 RU were immobilized. Unless otherwise noted, capture was performed for 180 s, and binding, dissociation, and regeneration steps were 120 s each. The concentrations of the analytes varied according to interaction strength and measurement mode.

In vitro *SIM interaction assay*

The influence of the DARPins on the interaction between Smt3 and RNF4 was analyzed by pull-down assays. Streptavidin agarose beads (15 μL slurry per sample) were equilibrated with 50 mM HEPES pH 7.4, 50 mM NaCl, 1% (v/v) glycerol, 1% (v/v) Triton X-100, and loaded with 0.25 nmol of purified biotinylated $^{His\text{-}AVI}$Smt3 for 60-90 min at 4°C on a rotating wheel. After washing, blocking with 1 mg/mL BSA for 30 min at 4°C, and renewed washing, beads were incubated with 10 nmol of DARPin in 100 μL buffer for 30 min at 4°C on a rotation wheel. Subsequently, 1 nmol of purified RNF4 was added, and samples were incubated for another 60 min at 4°C on a rotation wheel. After renewed washing, bound proteins were eluted by addition of 15 μL 1x NuPage loading dye and heating the

samples at 95°C for 5 min. Eluted material was analyzed by SDS-PAGE and western blotting with anti-RNF4 antibodies and quantified using Image Studio™. Degradation products of RNF4 were included, and a background signal was subtracted from the total signal. Signals of RNF4 in the presence of Smt3-specific DARPins were plotted relative to the amount retained in the presence of control DARPin E3_5.

In vitro SUMOylation and deSUMOylation assays

All SUMOylation and deSUMOylation assays were performed in a buffer containing 40 mM HEPES pH 7.4, 50 mM NaCl, and 8 mM magnesium acetate. SUMOylation reactions were incubated at 30°C unless otherwise noted, deSUMOylation reactions at 20°C. Reactions were stopped by addition of SDS loading buffer and heating at 95°C for 5 min and analyzed by SDS-PAGE and Coomassie staining or western blotting.

PCNA SUMOylation

In vitro SUMOylation assays were performed with DNA-loaded PCNA essentially as described with minor modifications.[29] Briefly, reactions contained 50 nM ^{His}PCNA, 100 nM E1, 50 nM Ubc9^{His}, 1 μM $^{His\text{-}AVI}$Smt3, 25 nM Siz1(1-508), 2.5 nM of nicked plasmid DNA, 30 nM RFC complex, and 3 μM of DARPin, and were incubated for 1 h. Reactions were started by the addition of 1 mM ATP, and products were analyzed by western blotting with an anti-PCNA antibody.

Assembly of unanchored Smt3 chains

In vitro assembly of Smt3 chains was monitored using 100 nM E1, 50 nM Ubc9(K153R)^{His}, 1 μM $^{His\text{-}AVI}$Smt3, and 5 μM of DARPins. Where indicated, ^{His}Siz1(1-508) was present at 50 nM. Reactions were set up and briefly pre-incubated without E1, started by addition of E1 and transfer to 30°C. They were terminated by addition of SDS loading buffer and heating at 95°C for 5 min. Products were analyzed by SDS-PAGE and western blotting with an anti-Smt3 antibody.

SUMOylation of a RanGAP1 fragment

A FRET-based SUMOylation assay was performed at 20°C essentially as described.[33] Final concentrations in the reactions were 10 nM E1, 10 nM Ubc9(K153R)^{His}, 100 nM $^{His\text{-}CFP}$GAPtail, 100 nM $^{His\text{-}YFP}$Smt3(K11/15/19R), and 0.2 mg/mL BSA. The reaction buffer contained 40 mM HEPES pH 7.4, 8 mM magnesium acetate, 50 mM NaCl and 0.1% Tween 20. A master mix without E1 was prepared and distributed to a 384-well plate. Samples were pre-incubated for 10 min with an equimolar amount or a 10-fold molar excess of DARPin over Smt3. SUMOylation reactions were started by addition of 1 mM ATP to all except the control sample. Fluorescence was recorded every 30 s for 20 min in a Tecan Spark plate reader, using a 430 nm filter for excitation of CFP and 485 nm and 535 nm for recording emission of CFP and YFP, respectively. Data were analyzed using the Graphpad Prism software by dividing the YFP by the CFP fluorescence signal, normalizing them to the values at t=0 min and subtracting the value of a control reaction without ATP. Reaction products were analyzed by western blotting with a rabbit anti-Smt3, and a mouse anti-GFP antibody. Blots were imaged with an Odyssey CLx system (LI-COR) using secondary antibodies tagged with near-infrared fluorophores (LI-COR Biosciences IRDye 680RD and 800CW, respectively).

DeSUMOylation

Ulp1 activity was followed using $^{His\text{-}Cys}$Smt3^{GFP} as a substrate. Substrate at 4 μM was pre-incubated for 10 min at 4°C with a 5-fold molar excess of the respective DARPin. After addition of 50 nM Ulp1, the reaction was incubated at 20°C and samples were taken at 1, 2, and 5 min. Products were analyzed by SDS-PAGE and Coomassie staining.

In vitro thioester assays

Thioester formation of Smt3 with E1 and E2 was analyzed at 30°C in reactions containing 5 μM Smt3 and a five-fold molar excess of DARPins in the same buffer as used for the SUMOylation assays. Reactions were terminated by adding a 3-fold concentrated denaturing loading buffer (8 M urea, 5% (w/v) SDS, 200 mM Tris-HCl pH 6.8, 1 mM EDTA, 0.1% (w/v) bromophenol blue) without heating, followed by SDS-PAGE and Coomassie staining. Control samples were incubated with loading buffer containing 50 mM DTT to reduce all thioesters.

E1 thioester

$^{His\text{-}AVI}$Smt3 and DARPins were pre-incubated on ice for 10 min before addition of 500 nM E1 and 1 mM ATP in reaction buffer. Samples were taken after 0, 5, and 15 min. Gel images were quantified using Image Studio software. Relative E1 thioester signals were determined from the ratio of thioester to total E1 signal, normalized against the signal of a sample treated with reducing agent.

E2 thioester

$^{His\text{-}AVI}$Smt3(K11/15/19R) was pre-incubated with 500 nM E1 and 1 mM ATP for 15 min in reaction buffer. DARPins were then added, and samples were incubated for 10 min. Finally, 750 nM Ubc9(K153R)^{His} was added, and samples were taken after 0, 5, and 10 min.

Crystallization of DARPin·SMT3 complexes

Prior to crystallization, DARPin·Smt3(20-98) complexes were purified by incubating the two proteins in a 1:1 molar ratio for 30 min on ice and subjecting them to gel filtration in a buffer containing 40 mM HEPES pH 7.4, 50 mM NaCl, and 1mM DTT. Peak fractions were pooled and concentrated to 20 mg/mL. Initial screening was done in a 96-well plate using the mosquito crystal robot (SPT Labtech). Crystal optimization took place in a 24-well plate using the hanging drop method.

Crystals of the A10·Smt3 complex formed at 20°C using a hanging drop setup with a reservoir solution containing 0.1 M Bis-Tris pH 6.5 and 23% (v/v) PEG 3350. The protein solution at 5 mg/mL was mixed in volume ratios of 2:1, 1:1, or 0.5:1 with the reservoir

solution. Crystals were cryo-protected with 0.1 mM Bis-Tris pH 6.5, 23% (v/v) PEG 3350, and 10% (v/v) PEG 200. The A10·Smt3 crystals belong to space group $P2_12_12_1$ with two A10·Smt3 complexes per asymmetric unit and unit cell constants a=42.97 Å, b=94.75 Å, c=120.96 Å.

The C10·Smt3 complex crystallized at 20°C in a reservoir solution containing 0.1 M Bis-Tris pH 6.5 and 16% (v/v) PEG 3350. The protein solution at 20 mg/mL was mixed in volume ratios of 2:1, 1.5:1, or 1:1 with reservoir solution. Crystals were cryo-protected with 0.1 mM Bis-Tris pH 6.5, 16% (v/v) PEG 3350 and 10% (v/v) PEG 200. The C10·Smt3 crystals belong to space group $C2_1$ with one C10·Smt3 complex per asymmetric unit and unit cell constants a=90.46 Å, b=44.69 Å, c=47.60 Å, b = 98.76 °.

Data collection, structure determination, and refinement

A 2.51 Å data set was collected from a A10·Smt3 crystal at SLS X06DA (PSI, Switzerland) and a 2.64 Å data set was collected from a C10·Smt3 crystal at SLS X06SA. All data sets were processed using XDS[67] and evaluated using the half-set correlation in the highest resolution shell. Both data sets were subjected to POINTLESS,[68,69] then AIMLESS[69,70] for data scaling. Structures were solved by molecular replacement using Phaser[71] within the PHENIX[72] or CCP4[69] package. For the A10·Smt3 structure, Smt3 (PDB: 1EUV) was used as search model, and Buccaneer[73] was used to build initial model of the DARPin A10. For the C10·Smt3 structure, DARPin E3_5 (PDB: 1MJ0) was used as search model, and Buccanneer was used to build an initial Smt3 model. Additional manual model building was done by Coot,[74] refinement was carried out by Refmac[69,75] and PHENIX.[72,76]

The A10·Smt3 complex structure has R_{work}/R_{free} values of 0.240/0.299 and the C10·Smt3 has R_{work}/R_{free} values of 0.232/0.288. The A10·Smt3 structure consists of 456 amino acids (Smt3 E21-Q95, DARPin A10 D15-L167) and 56 water molecules. Due to lack of electron density on their side chains, 32 amino acids were refined as alanine residues, but none of them are in the interaction region. The structure has 95.98% Ramachandran favored main chain torsion angles and no residues are outliers. The C10·Smt3 complex structure consists of 199 amino acids (Smt3 E21-I96, DARPin C10 S14-Q136) and 31 water molecules. Due to lack of electron density on their side chains, 13 amino acids were refined as alanine residues, but none of them are in the interaction region. The Ramachandran Plot depicts 96.41% of the main chain torsion angles in the most favored regions, 0.51% are marked as outliers. Interfaces were analyzed using PDBe PISA v1.52.[77] Images were generated in the PyMOL Molecular Graphics System, Version 2.5.8, Schrödinger, LLC.

Manipulation of budding yeast

Preparation of cell extracts

Denatured extracts for analysis by western blotting were prepared by trichloroacetic acid precipitation as described.[90]

Determination of growth curves

Exponentially growing cultures were diluted into a 96-well plate to an OD_{600} of 0.0125 in 200 μL of SC-complete medium containing 2 μg/mL doxycycline. Proliferation was monitored using a TECAN Spark 20M multimode microplate reader at 30°C for 20 h at a wavelength of 600 nm and a bandwidth of 3.5 nm. A well of medium not inoculated with a yeast culture (blank) served as control.

Cell cycle analysis

Ca. $1.5 \cdot 10^7$ cells were harvested and fixed for 10 min at room temperature in 2.5% (v/v) formaldehyde in 0.1 M potassium phosphate pH 6.4. After washing twice in potassium phosphate pH 6.6, and once in potassium phosphate pH 7.4, cells were permeabilized in 1 mL 70% (v/v) ethanol for 10 min at room temperature. Cells were pelleted, washed twice with 50 mM sodium citrate pH 7.0, and treated with 800 μg of RNase A in 1 mL citrate buffer for 1 h at 50°C. Samples were then washed once with citrate buffer, and propidium iodide was added to 32 μg/mL in citrate buffer. Samples were briefly sonicated and analyzed on an LSRFortessa SORP (BD Biosciences) flow cytometer equipped with BD FACSDIVA software. Data were analyzed using the FlowJo v10 software (FlowJo, LLC). Gates were applied for GFP-positive single cells to determine their DNA content.

Fluorescence microscopy

For live cell microscopy, 200 μL of an exponential culture were plated onto a concanavalin A-coated chambered glass-bottom coverslip (Ibidi), washed three times with medium, and released into fresh prewarmed SC-medium (30°C) supplemented with doxycycline and/or other drugs as required. Imaging was performed in an environmental control chamber at 30°C, using a DeltaVision Elite widefield microscope (GE Healthcare) equipped with a 60x oil immersion objective (NA=1.42), InsightSSITM solid-state illumination, Scientific CMOS camera, SoftWoRxTM software, and a built-in deconvolution algorithm. Z stacks with 21 steps (step size = 0.2 mm) were acquired for each image. Fluorescent proteins or dyes were imaged with their optimized filters. Differential interference contrast (DIC) was used for whole-cell images. The built-in deconvolution algorithm was used to reconstruct images.

For immunofluorescence, cells from an exponential culture were fixed with 0.1 volumes of a 37% (v/v) formaldehyde solution for 15-20 min at room temperature. 10 mL were harvested and resuspended in a potassium phosphate buffer (pH 6.4) containing 3.7% formaldehyde and incubated for 15 min at room temperature, followed by several washes with 0.1 M potassium phosphate and subsequently with spheroplasting buffer (0.1 M potassium phosphate pH 7.4, 1.2 M sorbitol, 0.5 mM $MgCl_2$). Zymolyase T100 was added for spheroplasting. Spheroplasts were immobilized on a poly-Lysine-coated slide for 15 min, followed by fixation in ice-cold methanol for 3 min and in ice-cold acetone for 10 s. After drying, all incubations were done in a wet chamber. Slides were blocked for 30 min with 1% (w/v) BSA in PBS, incubated with the primary antibody in PBS-BSA for 1 h, washed four times with PBS-BSA, incubated with the secondary antibody for 1 h, washed again, and subjected to DAPI staining (1:10,000 of a 0.1 mg/mL solution) for 15 min. After addition of ProLong Diamond mounting medium, samples were sealed with coverslips and kept at 4°C in the dark until imaging as described above.

For chromatin spreads, cells corresponding to 10 OD_{600} were collected and inactivated with 0.1% sodium azide, followed by spheroplasting in sorbitol mix (1.2 M sorbitol, 100 mM potassium phosphate pH 6.5) with 0.4 mg/mL zymolyase 20T, washing once in MES stop solution (100 mM MES pH 6.4, 1 mM EDTA, 0.5 mM $MgCl_2$, 1 M sorbitol) and resuspension in 0.5 mL MES stop solution. To prepare spreads, 20 μL spheroplasts, 40 μL of fixing solution (4% paraformaldehyde, 3.4% sucrose), 80 μL of 1% Lipsol, and 80 μL of fixing solution were added sequentially to a clean coverslip with brief mixing by swirling between additions. Samples were spread on coverslips with a glass rod and left to dry overnight. Slides were washed with 0.4% Photo-Flo 200 in water and with PBS and then mounted in mounting medium with DAPI before imaging.

QUANTIFICATION AND STATISTICAL ANALYSIS

Statistical treatment of surface plasmon resonance data was performed using the Biacore Evaluation Software, assuming a 1:1 interaction model. FRET signals, optical densities for growth curves and western blot signals were quantified from a minimum of three replicates, and mean values and standard deviations were calculated using Excel or GraphPad. Numbers of replicates and statistical treatments are provided in the figure and table legends.